

## RHIC Run 22, 9 o'clock, a Snake in the Blue

F. Méot

June 2022

Collider Accelerator Department  
**Brookhaven National Laboratory**

**U.S. Department of Energy**

USDOE Office of Science (SC), Nuclear Physics (NP) (SC-26)

Notice: This technical note has been authored by employees of Brookhaven Science Associates, LLC under Contract No. DE-SC0012704 with the U.S. Department of Energy. The publisher by accepting the technical note for publication acknowledges that the United States Government retains a non-exclusive, paid-up, irrevocable, world-wide license to publish or reproduce the published form of this technical note, or allow others to do so, for United States Government purposes.

## **DISCLAIMER**

This report was prepared as an account of work sponsored by an agency of the United States Government. Neither the United States Government nor any agency thereof, nor any of their employees, nor any of their contractors, subcontractors, or their employees, makes any warranty, express or implied, or assumes any legal liability or responsibility for the accuracy, completeness, or any third party's use or the results of such use of any information, apparatus, product, or process disclosed, or represents that its use would not infringe privately owned rights. Reference herein to any specific commercial product, process, or service by trade name, trademark, manufacturer, or otherwise, does not necessarily constitute or imply its endorsement, recommendation, or favoring by the United States Government or any agency thereof or its contractors or subcontractors. The views and opinions of authors expressed herein do not necessarily state or reflect those of the United States Government or any agency thereof.

# RHIC Run 22, 9 o'clock, a Snake in the Blue

F. Méot, E. Aschenauer, H. Huang, A. Marusic, V. Ptitsyn, V. Ranjbar, G. Robert-Demolaize, V. Schoefer

June 13, 2022

*Tech. Note C-A/AP/661*  
*BNL C-AD*

## Contents

5	<b>1 Introduction</b>	<b>3</b>
6	1.1 RHIC snakes . . . . .	3
7	1.2 9 o'clock 2-coil Blue snake . . . . .	4
8	1.3 Expected perturbation of the polarization . . . . .	5
9	<b>2 Orbits and spin across complete and 2-coil snakes</b>	<b>7</b>
10	2.1 Injection energy . . . . .	9
11	2.2 255 GeV . . . . .	9
12	<b>3 Polarization in RHIC Blue with 2-coil 9 o'clock snake</b>	<b>9</b>
13	3.1 Case of 1&4 coils 9 o'clock snake . . . . .	9
14	3.1.1 At injection ( $G\gamma = 45.5$ ) . . . . .	10
15	3.1.2 At 255 GeV . . . . .	12
16	3.1.3 $\nu_{sp} = 393 + \nu_Z$ crossing . . . . .	12
17	3.2 Case of 1&3 coils 9 o'clock snake . . . . .	14
18	3.2.1 At injection ( $G\gamma = 45.5$ ) . . . . .	14
19	3.2.2 At 255 GeV . . . . .	19
20	<b>4 Polarization in RHIC Blue, using Run 22 optics</b>	<b>21</b>
21	4.1 Snake spin matrices . . . . .	21
22	4.2 At injection ( $G\gamma = 45.5$ ) . . . . .	21
23	4.2.1 Injection optics . . . . .	21
24	4.2.2 Spin, at injection . . . . .	23
25	4.3 255 GeV optics ( $G\gamma = 487.253$ ) . . . . .	24
26	4.3.1 255 GeV optics . . . . .	24
27	4.3.2 Spin, at 255 GeV . . . . .	26
28	4.3.3 Scans of $\vec{n}_0$ components, at STAR, H-Jet, pC-Polarimeter . . . . .	28
29	<b>5 Polarization in RHIC Yellow with spin rotators, Run 22 optics</b>	<b>29</b>
30	5.1 At injection ( $G\gamma = 45.5$ ) . . . . .	29
31	5.2 At 255.200 GeV, $G\gamma = 487.635$ . . . . .	30
32	5.3 Add spin rotators . . . . .	31
33	5.4 Use spin rotators to manipulate spin $\vec{n}_0$ at STAR . . . . .	31
34	<b>6 Spin rotators</b>	<b>34</b>
35	6.1 Spin rotator field map . . . . .	34
36	<b>Appendix</b>	<b>36</b>
37	<b>A Optical sequences for 2-coil 9 o'clock and full 3 o'clock snakes</b>	<b>36</b>
38	<b>B Optical sequence of a spin rotator</b>	<b>37</b>

## 1 Introduction

The simulations detailed in this Tech. Note were aimed at determining new RHIC Blue 9 o'clock snake coil current and local closed orbit bump settings, together with updated - optimized - 3 o'clock snake settings, in order to recover from power supply dips which, early in the run (December 2021), caused the failure of 9 o'clock snake's second coil in a first occurrence, and of its fourth coil in addition in a second occurrence, leaving the poor animal with just its coils 1 and 3.

Documentation from a similar incident in Yellow in 2003 could be leaned on and allowed to promptly figure various necessary measures for swift recovery using the 9 o'clock Blue snake coils which survived the dip [1]. Reference [1] reports in particular that, in this 2003 incident, "[it was] decided to run the [failed] snake as a 88% partial snake while keeping the angles between the two snakes as 90° [...]. In general, the polarization level was not as good as Blue ring".

By contrast in this Run 22 incident, thorough simulations using the snake OPERA field maps helped determine new settings of the handicapped, 2-coil, Blue ring 9 o'clock snake currents and local closed orbit bump, and concurrently determine slight adjustment of the 3 o'clock snake currents, which allowed recovering full polarization at store, as good as could be expected from normal operation - even better over extended periods than in the Yellow ring, Fig. 1.

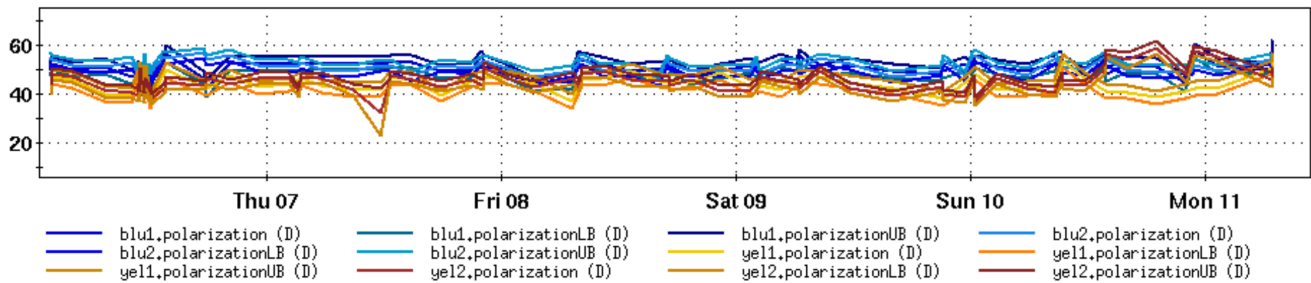


Figure 1: Sample polarization in Blue and Yellow rings during RHIC Run 22, over the period 4/6-11/2022

### 1.1 RHIC snakes

The representation of a complete snake using OPERA field maps of its four modules (Fig. 2) consists in a sequence of 4 maps [2]. Mechanically the four modules are essentially identical, however the 1 and 4 outer module field maps result from low field OPERA computation (100 A current), whereas the 2 and 3 inner module field maps result from high field computation (322 A current). The resulting 4-map series R+R-R+R- or R-R+R-R+ found in RHIC rings (Fig. 3) are as follows and determine the sign factors to apply to the OPERA maps:

sign to be applied		field map file name
9 o'clock, Blue(CW)	3 o'clock, Blue(CW)	
3 o'clock, Yell.(CCW)	9 o'clock, Yell.(CCW)	
(R+R-R+R-)	(R-R+R-R+)	
+	-	model3a2a - x - 4.4.y - 4.4.z - 180_180 - integral.table
-	+	model3a2a322a - x - 4.4.y - 4.4.z - 180_180 - integral.table
+	-	model3a2a322a - x - 4.4.y - 4.4.z - 180_180 - integral.table
-	+	model3a2a - x - 4.4.y - 4.4.z - 180_180 - integral.table

These OPERA maps are archived on C-AD computers at

`/rap/lattice_tools/zgoubi/RHICZgoubiModel/snakeFieldMaps/161216_secondSet_inclSingleHelix`

and as well in the sourceforge repository

`https://sourceforge.net/p/zgoubi/code/HEAD/tree/trunk/exemples/RHIC/snakesWithFieldMaps/fieldMaps/`

### RHIC rings frames, snake angles

In the present simulations, referring to Fig. 3 and using a direct trihedra (O;X,Y,Z): in RHIC Blue the moving frame is oriented clockwise, longitudinal axis (X) points in the direction of the motion, radial axis (Y) points outward, vertical axis (Z) points up; ray-tracing simulations show that consistency with snake axes orientations of Fig. 3 (at  $\pm 45^\circ$  from the X axis) requires OPERA field map currents for spin flip to be (details below and in [2])

$$9\text{'oclock snake: } \underbrace{+100 \quad -322 \quad +322 \quad -100}_{\text{snake axis at } -45^\circ}, \quad 3\text{'oclock snake: } \underbrace{-100 \quad +322 \quad -322 \quad +100}_{\text{snake axis at } +45^\circ}$$

which is consistent in turn with the R+R-R+R- and R-R+R-R+ sign series in Fig. 3.

Some parameters of RHIC snakes [2]:

A snake is a series of 4 right-handed helix modules (Fig. 2), a helix module is 2.4 m long, bore 10 cm (this matters regarding geometrical acceptance versus local closed orbit bump excursion), modules are spaced 0.212/0.448/0.212 m hence an overall length of 10.472 m. Field sign alternates from a module to the next

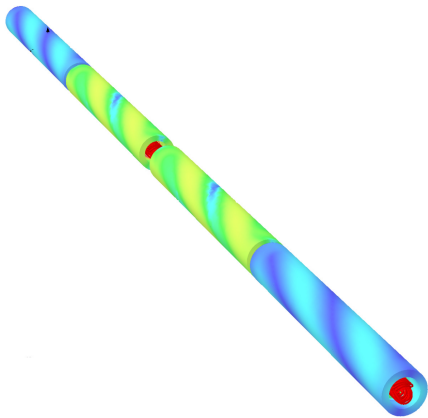


Figure 2: OPERA model of RHIC four helical module snake

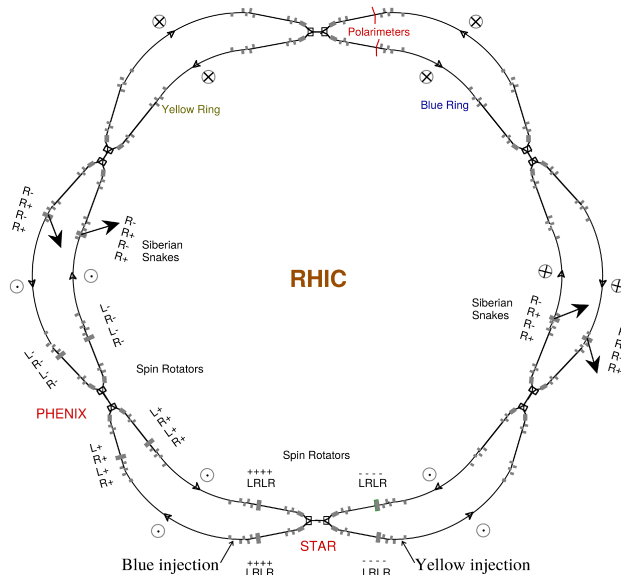


Figure 3: Locations of the helical snakes in RHIC Blue and Yellow rings, at 9 o'clock and 3 o'clock. Beam goes clockwise in Blue, counter-clockwise in Yellow

In a similar manner in RHIC Yellow, the sign series are, going CCW,

$$\begin{aligned}
 &3\text{'o'clock snake: } \underbrace{+100 \quad -322 \quad +322 \quad -100}_{\text{snake axis at } -45^\circ}, & 9\text{'o'clock snake: } \underbrace{-100 \quad +322 \quad -322 \quad +100}_{\text{snake axis at } +45^\circ}
 \end{aligned}$$

These two snake series found in RHIC Blue and Yellow only differ by the reversed field signs. Snake models for ray-tracing are available at

<https://sourceforge.net/p/zgoubi/code/HEAD/tree/trunk/exemples/RHIC/snakesWithFieldMaps/examples/snakes/>

55 The two files found there: R-R-R-R-Snake.inc and R-R+R-R+Snake.inc, are equipped with a matching procedure which ensures proper entrance coordinates for orbit centering in the snake (Fig. 4).

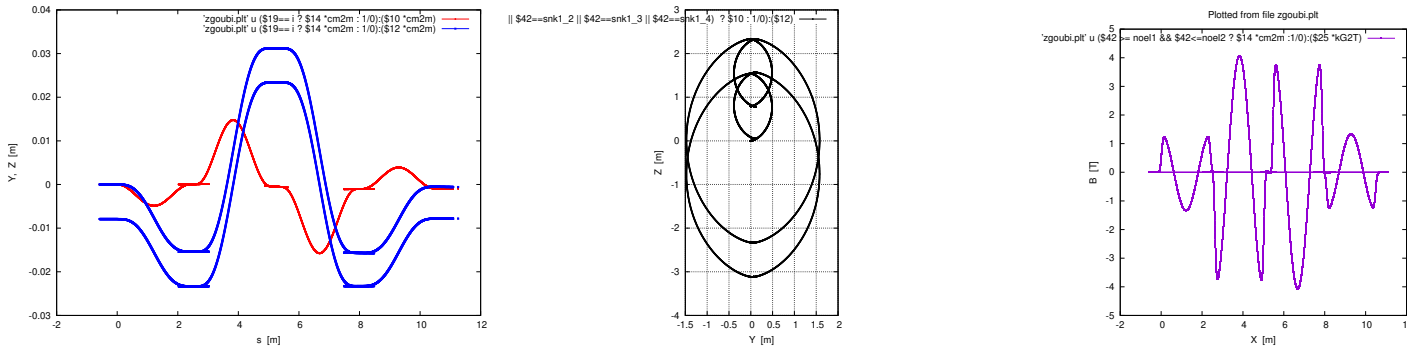


Figure 4: Orbit centering through the R+R-R+R- series. Two cases are displayed: some arbitrary dose of off-centering, starting point for the matching, and centered after matching. Left: Y(s) and Z(s) orbits along the snake; middle: (Y,Z) projected helical motion; right: field B<sub>Z</sub>(s) along the orbit, largely independent of possible mis-centering of the helix

56

### 1.2 9 o'clock 2-coil Blue snake

**Coil 1&4 snake** Following the first power supply dip, a configuration using coils 1&4 was assessed to bring RHIC Blue 9 o'clock snake back to life, with supply current in the high-field 300 A region, thus a high field map was substituted to coils 1 and 4 low field ones, resulting

57

in the modified sequence

sign applied (R-00R+)	field map
–	<code>b_model3a2a322a - x - 4.4.y - 4.4.z - 180.180 - integral.table</code>
field set to 0	<code>b_model3a2a322a - x - 4.4.y - 4.4.z - 180.180 - integral.table</code>
field set to 0	<code>b_model3a2a322a - x - 4.4.y - 4.4.z - 180.180 - integral.table</code>
+	<code>b_model3a2a322a - x - 4.4.y - 4.4.z - 180.180 - integral.table</code>

58 Note that, compared to the 9 o'clock complete (4-coil) snake, current supply signs are reversed in order to obtain proper spin rotation  
59 properties, this is further addressed in the next sections.

A model is available at

<https://sourceforge.net/p/zgoubi/code/HEAD/tree/trunk/exemples/RHIC/snakesWithFieldMaps/examples/snakes/>

60 The file found there: R-00R+\_9oclockBlueSnake.inc, ensures the matching of entrance coordinates for orbit centering in the snake.

**Coil 1&3 snake** Following the second power supply dip, there was no other possibility than using coils 1 and 3, with supply current in the 300 A region as well, thus the following configuration,

sign applied (R-0R+0)	field map
–	<code>b_model3a2a322a - x - 4.4.y - 4.4.z - 180.180 - integral.table</code>
field set to 0	<code>b_model3a2a322a - x - 4.4.y - 4.4.z - 180.180 - integral.table</code>
+	<code>b_model3a2a322a - x - 4.4.y - 4.4.z - 180.180 - integral.table</code>
field set to 0	<code>b_model3a2a - x - 4.4.y - 4.4.z - 180.180 - integral.table</code>

A model of this R-0R+0 two-coil snake is available at

<https://sourceforge.net/p/zgoubi/code/HEAD/tree/trunk/exemples/RHIC/snakesWithFieldMaps/examples/snakes/>

61 The file found there: R-0R+0\_9oclockBlueSnake.inc, ensures the matching of entrance coordinates for orbit centering in the snake (Fig. 5),  
this is detailed in the next sections.

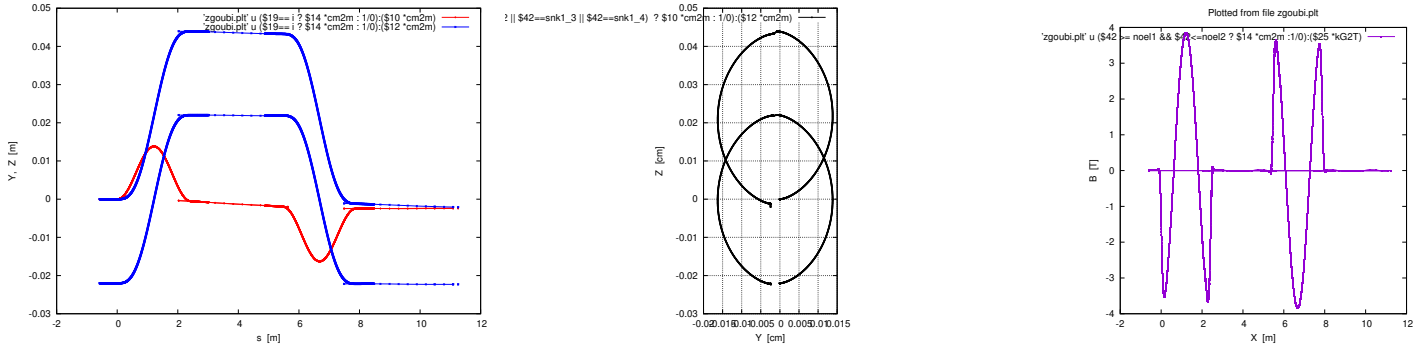


Figure 5: Typical orbit centering through the R-0R+0 series. On each graph two cases are displayed: (i) some arbitrary dose of off-centering, starting point for the matching, and (ii) centered after matching. Left: Y(s) and Z(s) orbits along the snake; middle: (Y,Z) projected helical motion; right: field  $B_Z(s)$  along the orbit, essentially independent of the mis-centering of the latter

62

### 63 1.3 Expected perturbation of the polarization

64 Here we assess the effect on spin tune and on polarization, of a perturbation of the spin precession angle in 9 o'clock snake.

65 A rotation  $T(\theta_2 \leftarrow \theta_1)$  of a spinor  $\psi = \begin{pmatrix} \psi_1 \\ \psi_2 \end{pmatrix}$ , over an orbital interval  $[\theta_1, \theta_2]$ , by an angle  $\phi$  around a unitary rotation axis  $\vec{\omega} \begin{pmatrix} \omega_Y \\ \omega_X \\ \omega_Z \end{pmatrix}$   
66 (Y, X, Z respectively radial, longitudinal, vertical) can be expressed under the form [3]

$$\psi(\theta_2) = T(\theta_2 \leftarrow \theta_1) \psi(\theta_1) = \underbrace{e^{\frac{i}{2}(\vec{\omega} \cdot \vec{\sigma}) \phi}}_{\text{a } 2 \times 2 \text{ matrix}} \psi(\theta_1) = \left[ I \cos \frac{\phi}{2} + i(\vec{\omega} \cdot \vec{\sigma}) \sin \frac{\phi}{2} \right] \psi(\theta_1) \quad (1)$$

I is the identity matrix and  $\vec{\sigma} = \begin{pmatrix} \sigma_Y \\ \sigma_X \\ \sigma_Z \end{pmatrix}$  with

$$\sigma_Y = \begin{pmatrix} 0 & 1 \\ 1 & 0 \end{pmatrix}, \sigma_X = \begin{pmatrix} 0 & -i \\ i & 0 \end{pmatrix}, \sigma_Z = \begin{pmatrix} 1 & 0 \\ 0 & -1 \end{pmatrix}$$

the Pauli matrices.

Observing just upstream of 9 o'clock snake the sector sequence is (with snake 1 - respectively 2 - the first - resp. 2nd - snake met from the injection, Fig. 3)

$$\text{snake 1} \rightarrow \pi \rightarrow \text{snake 2} \rightarrow \pi$$

yielding

$$T_{1\text{-turn}} = e^{\frac{i}{2}(\vec{\omega}_Z \cdot \vec{\sigma})G\gamma\pi} \times e^{\frac{i}{2}(\vec{\omega}_{\text{sn}2} \cdot \vec{\sigma})\pi} \times e^{\frac{i}{2}(\vec{\omega}_Z \cdot \vec{\sigma})G\gamma\pi} \times e^{\frac{i}{2}(\vec{\omega}_{\text{sn}1} \cdot \vec{\sigma})\pi}$$

wherein

$$\begin{aligned} \vec{\omega}_Z \cdot \vec{\sigma} &= \sigma_Z, \\ \vec{\omega}_{\text{sn}1} \cdot \vec{\sigma} &= \begin{pmatrix} -\frac{\sqrt{2}}{2} \\ \frac{\sqrt{2}}{2} \\ 0 \end{pmatrix} \cdot \vec{\sigma} = -\frac{\sqrt{2}}{2}\sigma_Y + \frac{\sqrt{2}}{2}\sigma_X, \\ \vec{\omega}_{\text{sn}2} \cdot \vec{\sigma} &= \begin{pmatrix} \frac{\sqrt{2}}{2} \\ \frac{\sqrt{2}}{2} \\ 0 \end{pmatrix} \cdot \vec{\sigma} = \frac{\sqrt{2}}{2}\sigma_Y + \frac{\sqrt{2}}{2}\sigma_X \end{aligned} \quad (2)$$

so yielding

$$T_{1\text{-turn}} = e^{\frac{i}{2}\sigma_Z G\gamma\pi} \times e^{\frac{i}{2}\frac{\sqrt{2}}{2}(\sigma_Y + \sigma_X)\pi} \times e^{\frac{i}{2}\sigma_Z G\gamma\pi} \times e^{\frac{i}{2}\frac{\sqrt{2}}{2}(-\sigma_Y + \sigma_X)\pi}$$

which can be written under the equivalent form [3]

$$T_{1\text{-turn}} = \frac{1}{2} \left( I \cos \frac{G\gamma\pi}{2} + i\sigma_Z \sin \frac{G\gamma\pi}{2} \right) \times (\sigma_Y + \sigma_X) \times \left( I \cos \frac{G\gamma\pi}{2} + i\sigma_Z \sin \frac{G\gamma\pi}{2} \right) \times (-\sigma_Y + \sigma_X)$$

Expanding, this results in

$$T_{1\text{-turn}} = i\sigma_Z$$

equivalent to  $(I \cos \frac{\pi}{2} + i\sigma_Z \sin \frac{\pi}{2})$ , a  $\phi = \pi$  angle,  $Z$ -axis rotation. Introduce in snake 1 a rotation angle defect  $\delta$ , with  $2 \times 2$  matrix

$$T_\delta = I \cos \frac{\delta}{2} - i \frac{\sqrt{2}}{2} (\sigma_Y - \sigma_X) \sin \frac{\delta}{2}$$

yielding (with observation point upstream of the defect)

$$T_{1\text{-turn}} \times T_\delta = i\sigma_Z \cos \frac{\delta}{2} + i \frac{\sqrt{2}}{2} (\sigma_X + \sigma_Y) \sin \frac{\delta}{2}$$

The spin tune satisfies

$$\cos \pi \nu_{\text{sp}} = \frac{1}{2} \text{Trace}(T_{1\text{-turn}} \times T_\delta) = 0 \quad \Rightarrow \quad \nu_{\text{sp}} = \frac{1}{2}$$

The spin eigenvector is

$$\vec{\omega}_\pm = \frac{(\pm)}{\sqrt{1 - t_{0,1\text{-turn}}^2}} \begin{pmatrix} t_{Y,1\text{-turn}} \\ t_{X,1\text{-turn}} \\ t_{Z,1\text{-turn}} \end{pmatrix} \quad (3)$$

wherein

$$t_{0,1\text{-turn}} = (T_{11} + T_{22})/2, \quad t_{Y,1\text{-turn}} = (T_{12} + T_{21})/2i, \quad t_{X,1\text{-turn}} = (T_{12} - T_{21})/2, \quad t_{Z,1\text{-turn}} = (T_{11} - T_{22})/2i$$

and the  $T_{ij}$  are the four components of the  $T_{1\text{-turn}} \times T_\delta$  matrix. Identifying yields

$$t_0 = 0, \quad t_Y = t_X = \frac{\sqrt{2}}{2} \sin \frac{\delta}{2}, \quad t_Z = \cos \frac{\delta}{2}$$

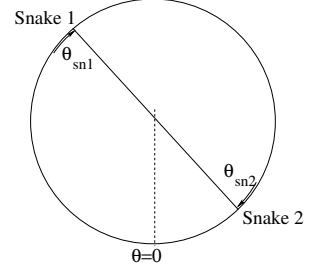
hence the eigenvector, just upstream of 9 o'clock snake

$$\vec{\omega} = \begin{pmatrix} \frac{\sqrt{2}}{2} \sin \frac{\delta}{2} \\ \frac{\sqrt{2}}{2} \sin \frac{\delta}{2} \\ \cos \frac{\delta}{2} \end{pmatrix} \approx \begin{pmatrix} \frac{\sqrt{2}}{2} \frac{\delta}{2} \\ \frac{\sqrt{2}}{2} \frac{\delta}{2} \\ 1 - \frac{\delta^2}{8} \end{pmatrix} \quad (4)$$

Thus the local spin precession vector  $\vec{\omega}$  is at an angle  $\delta/2$  (half the defect value) to the vertical axis. With  $\delta \lesssim 20^\circ \approx 350 \text{ mrad}$  (based on the present simulations, next Sections), that sets the vertical component of the spin precession axis at

$$\omega_Z \approx 0.98$$

i.e., about 2% polarization loss assuming vertical spin injection.



A sketch of snake configuration in RHIC. The origin  $\theta = 0$  is taken at IP6; 9 o'clock and 3 o'clock snakes are respectively  $\theta_{\text{sn}1}$  and  $\theta_{\text{sn}2}$  away.



## 2 Orbits and spin across complete and 2-coil snakes

Inspection of orbit geometry and spin precession in snakes proper is required prior to installing them in the computer model of RHIC Blue lattice. The field in the snakes is maintained constant during acceleration (Figs. 8, 12, 16), thus orbit perturbation culminates at injection energy. Spin motion - flipping - is essentially independent of energy (Figs. 9, 13, 17).

The left column below (Figs. 6-9) shows the orbit geometry and the field and spin motion along the orbit, in the regular, 4-coil, 9 o'clock snake; the central column (Figs. 10-13) shows the case of coils 1&4; the right column (Figs. 14-17) shows the case of coils 1&3. These data are obtained by ray-tracing through the field maps. Orbits have been centered, as happens in RHIC ring. The snake models introduced in Secs. 1.1 and 1.2 are used in Figs. 6-17 simulations.

**Complete 4-module 9 o'clock snake,  
100/-322/322/-100 Amp**

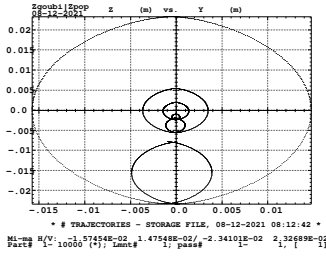


Figure 6: YZ projection of orbits at 255, 100 and 23 GeV.

**1&4 coil snake,  
-300/0/0/+300 Amp**

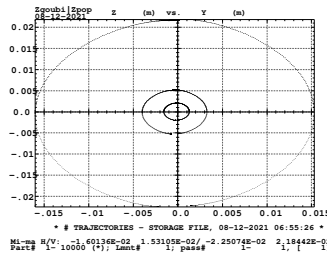


Figure 10: YZ projection of orbits at 255, 100 and 23 GeV.

**1&3 coil snake,  
-320/0/+320/0 Amp**

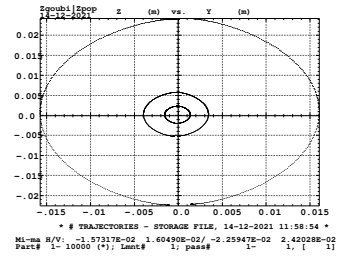


Figure 14: YZ projection of orbits at 255, 100 and 23 GeV.

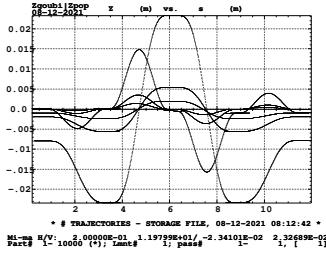


Figure 7: Y(s) and Z(s) orbits.

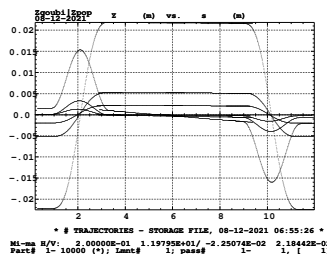


Figure 11: Y(s) and Z(s) orbits.

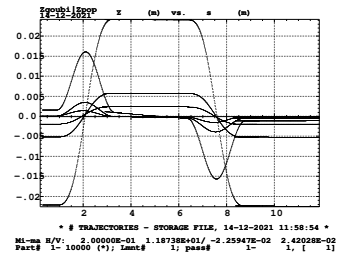


Figure 15: Y(s) and Z(s) orbits.

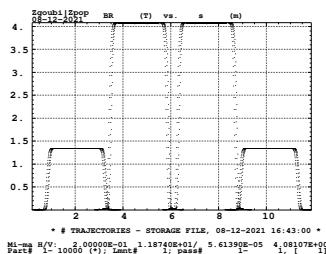


Figure 8:  $|B(s)|$  - field along orbits.

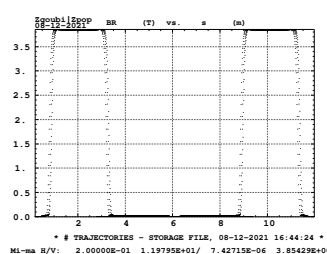


Figure 12:  $|B(s)|$  - field along orbits.

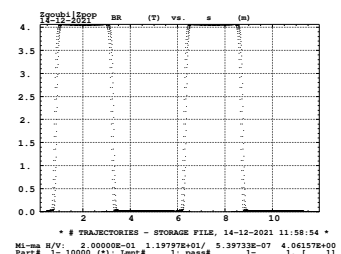


Figure 16:  $|B(s)|$  - field along orbits.

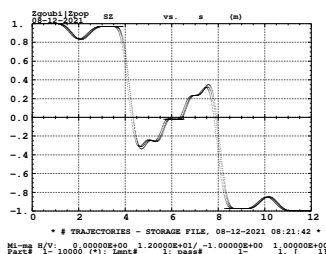


Figure 9:  $S_Z(s)$ .

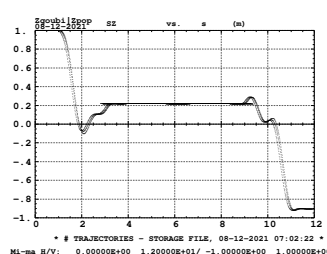


Figure 13:  $S_Z(s)$ .

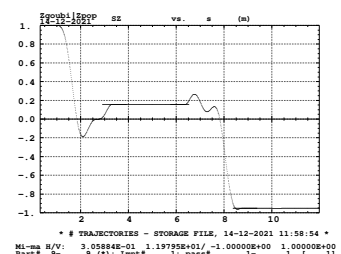


Figure 17:  $S_Z(s)$ .

## 72 Time of flight

73 The TOF along the helical orbit across the snake, a necessary quantity for tuning the RF frequency at injection, is given in Tab. 1 for the three  
74 different settings shown in Figs 7, 11, 15 and an additional -311/0/0/+311 Amp, coil 1&4 case.

Table 1: Time of flight on the helical orbit across 9 o'clock snake. The X-projected extent is 12.036 meters in all cases

	$\mu\text{S}$		
	255 GeV	100 GeV	23 GeV
Complete snake:			
	4.01480966E-02	4.01498453E-02	4.01850617E-02
Coil 1&4 snake:			
311A	4.01480937E-02	4.01498270E-02	4.01847290E-02
300A	4.01480909E-02	4.01498090E-02	4.01844007E-02
Coil 1&3 snake:			
320A	4.01480960E-02	4.01498419E-02	4.01849990E-02

TOF values in Tab. 1 account for extra end drift sections which are introduced for reasons of geometry consistency with the MADX model, given that the overall length of a 4-field map sequence exceeds the actual length of the snake 4-module magnet. In a practical manner in these simulations a snake insertion is 12.036 m long, including short drift sections at the extremities, and negative drifts in between for field map positioning, as follows for instance in the case of the R+R-R+R- series:

```
'DRIFT'
3.600000
'DRIFT'
16.400000
'TOSCA'   snk_pmpm_lowB
+1.  1.  1.  1.
b_model13a2a-x-4_4_y-4_4_z-180_180-integral.table
'DRIFT'
-98.800000
'TOSCA'   snk_pmpm_highB
-1.  1.  1.  1.
b_model13a2a322a-x-4_4_y-4_4_z-180_180-integral.table
'DRIFT'   VMON       pmpm_B7.1           ! Center of snake.
-37.6
'DRIFT'
-37.6
'TOSCA'   snk_pmpm_highB
+1.  1.  1.  1.
b_model13a2a322a-x-4_4_y-4_4_z-180_180-integral.table
'DRIFT'
-98.800000
'TOSCA'   snk_pmpm_lowB
-1.  1.  1.  1.
b_model13a2a-x-4_4_y-4_4_z-180_180-integral.table
'DRIFT'
16.400000
'DRIFT'
-78.200000
'MARKER'  R+R-R+R-Snake_E
```

## 75 Spin matrices

76 It results from the simulations - detailed below - that both complete and 2-coil and snakes have spin matrix close to  $\begin{pmatrix} 0 & -1 & 0 \\ -1 & 0 & 0 \\ 0 & 0 & -1 \end{pmatrix}$ ,

77 which corresponds to near 100% snake,  $\approx 180^\circ$  precession, around an axis at  $\approx -45^\circ$ :

78 - with  $\phi = 180^\circ$  spin precession, snake spinor rotations write (see Sec. 1.3),

$$T_{\text{snk}} \equiv \begin{pmatrix} t_0 + it_Z & t_X + it_Y \\ -t_X + it_Y & t_0 - it_Z \end{pmatrix} = \frac{\sqrt{2}}{2} \begin{pmatrix} 0 & 1 + \epsilon i \\ -1 + \epsilon i & 0 \end{pmatrix}$$

79 wherein  $\epsilon = \pm 1$  for respectively  $\pm 45^\circ$  axis;

- in 3D space, and by identification of the  $t_{0,x,s,y}$  terms, this yields the spin rotation matrix

$$R \equiv \begin{pmatrix} t_0^2 + t_Y^2 - t_X^2 - t_Z^2 & 2(t_Y t_X + t_0 t_Z) & 2(t_Y t_Z - t_0 t_X) \\ 2(t_Y t_X - t_0 t_Z) & t_0^2 - t_Y^2 + t_X^2 - t_Z^2 & 2(t_X t_Z + t_0 t_Y) \\ 2(t_Y t_Z + t_0 t_X) & 2(t_X t_Z - t_0 t_Y) & t_0^2 - t_Y^2 - t_X^2 + t_Z^2 \end{pmatrix} = \begin{pmatrix} 0 & \pm 1 & 0 \\ \pm 1 & 0 & 0 \\ 0 & 0 & -1 \end{pmatrix}, \text{ qed.}$$

80 The 3 o'clock snake axis in these simulations is at +45 deg from the longitudinal axis.

## 2.1 Injection energy

### Complete snake +100/-322/322/-100:

```
Spin matrix, momentum group # 3 :
2.452685E-02  -0.999220  -3.094373E-02
-0.999210    -2.353451E-02 -3.203606E-02
3.128283E-02  3.170501E-02  -0.999008

Determinant = 1.0000000000
Trace = -0.9980152480 ; spin precession = 177.4472300590 deg
Precession axis : ( 0.7156, -0.6986, 0.0001)
```

### Case 1-4 coils -322/0/0/+322:

```
Spin matrix, momentum group # 3 :
-0.118267  -0.967760  0.222380
-0.967849  0.162413  0.192071
-0.221996  -0.192515  -0.955854

Determinant = 1.0000000000
Trace = -0.9117071437 ; spin precession = 162.9118039104 deg
Precession axis : (-0.6544, 0.7561, -0.0002)
```

### Case 1-4 coils -311/0/0/+311:

```
Spin matrix, momentum group # 3 :
1.891284E-02  -0.967921  0.250544
-0.967999    4.499225E-02  0.246889
-0.250242    -0.247195  -0.936095

Determinant = 1.0000000000
Trace = -0.8721897918 ; spin precession = 159.4057590078 deg
Precession axis : (-0.7023, 0.7119, -0.0001)
```

### Case 1-4 coils -300/0/0/+300:

```
Spin matrix, momentum group # 1 :
0.159524  -0.946288  0.281230
-0.946295  -6.542902E-02  0.316616
-0.281209  -0.316634  -0.905905

Determinant = 1.0000000000
Trace = -0.8118102368 ; spin precession = 154.9454645073 deg
Precession axis : (-0.7477, 0.6641, -0.0000)
```

### Case 1-3 coils -320/0/+320/0:

```
Spin matrix, momentum group # 1 :
-9.294294E-02  -0.969268  0.227774
-0.969313    0.140372  0.201812
-0.227583    -0.202027  -0.952571

Determinant = 1.0000000000
Trace = -0.9051412857 ; spin precession = 162.2828892840 deg
Precession axis : (-0.6635, 0.7482, -0.0001)
```

## 2.2 255 GeV

### Complete snake +100/-322/322/-100:

```
Spin matrix, momentum group # 1 :
3.214335E-02  -0.999077  -2.848681E-02
-0.999072    -3.129976E-02 -2.958057E-02
2.866164E-02  2.941120E-02  -0.999156

Determinant = 1.0000000000
Trace = -0.9983127948 ; spin precession = 177.6463758024 deg
Precession axis : ( 0.7182, -0.6958, 0.0001)
```

### Case 1-4 coils -322/0/0/+322:

```
Spin matrix, momentum group # 1 :
-0.109159  -0.967942  0.226213
-0.967952  0.155286  0.197372
-0.226172  -0.197418  -0.953872

Determinant = 1.0000000000
Trace = -0.9077445293 ; spin precession = 162.5296174298 deg
Precession axis : (-0.6575, 0.7534, -0.0000)
```

### Case 1-4 coils -311/0/0/+311:

```
Spin matrix, momentum group # 1 :
2.657882E-02  -0.966760  0.254300
-0.966768    3.984734E-02  0.252530
-0.254269    -0.252562  -0.933574

Determinant = 1.0000000000
Trace = -0.8671476616 ; spin precession = 158.9989455087 deg
Precession axis : (-0.7047, 0.7095, -0.0000)
```

### Case 1-4 coils -300/0/0/+300:

```
Spin matrix, momentum group # 1 :
0.159352  -0.946312  0.281247
-0.946318  -6.526478E-02  0.316580
-0.281228  -0.316597  -0.905912

Determinant = 1.0000000000
Trace = -0.8118245635 ; spin precession = 154.9464337062 deg
Precession axis : (-0.7476, 0.6641, -0.0000)
```

### Case 1-3 coils -320/0/+320/0:

```
Spin transfer matrix, momentum group # 1 :
-8.426618E-02  -0.969199  0.231413
-0.969243    0.133617  0.206673
-0.231228    -0.206879  -0.950649

Determinant = 1.0000000000
Trace = -0.9012988965 ; spin precession = 161.9246766405 deg
Precession axis : (-0.6664, 0.7456, -0.0001)
```

## 3 Polarization in RHIC Blue with 2-coil 9 o'clock snake

RHIC Run 17 pp11-v7 optics was used in a first approach, for practical reasons; it anyway provides principle results which hold for Run 22 optics (RHIC Run 22 optics proceeds from cloning of RHIC pp11-v7).

The simulations in this Section indicate that

(i) the local closed orbit bump should be given a non-zero, positive, incidence at entrance of 9 o'clock snake, in order to overcome the adverse effect of the larger helix radius at the ends of the snake compared to the regular 4-coil operation case (about two times greater, compare Fig. 6 and Figs. 10, 14, p. 7), with a subsequent large kick of the vertical orbit in BI9\_QF7 quadrupole;

(i) 9 o'clock 2-coil snake has to be operated as near-full snake (near-180 deg precession; this will prove doable, current-wise);

(ii) an additional slight adjustment of 3 o'clock snake allows full recovery of beam polarization (Fig. 1).

### 3.1 Case of 1&4 coils 9 o'clock snake

Operating RHIC Blue 9 o'clock snake with just its coils 1 and 4 was investigated first, following the loss of coil 2 (on Dec. 3, following from a lab-wide power outage).

Orbit and spin data across the snakes in these simulations are as displayed in Figs. 10-13 (p. 7). Changing snake 1 from 4- to 2-coil, changes tunes slightly and chromaticities substantially more; both quantities are re-tuned to the MADX model values (this requires marginal QF and QD family quad strength changes, and a little more substantial SXF and SXF sextupole family strength changes).

Changing the current in 9 o'clock snake in the process of finding an optimum setting, changes slightly the helical orbit and the optics (betatron tunes, etc.). These effects are not corrected as they have marginal impact on spin eigenvectors and spin tune, in particular no correction is applied in simulations involving snake current scans.

### 3.1.1 At injection ( $G\gamma = 45.5$ )

Figures 18, 19 show the optics used. Note the following: (i) IP separation bumps have been zero-ed here, (ii) a greater vertical closed orbit excursion in 9 o'clock snake, compared to 3 o'clock, results from its 2-coil operation.

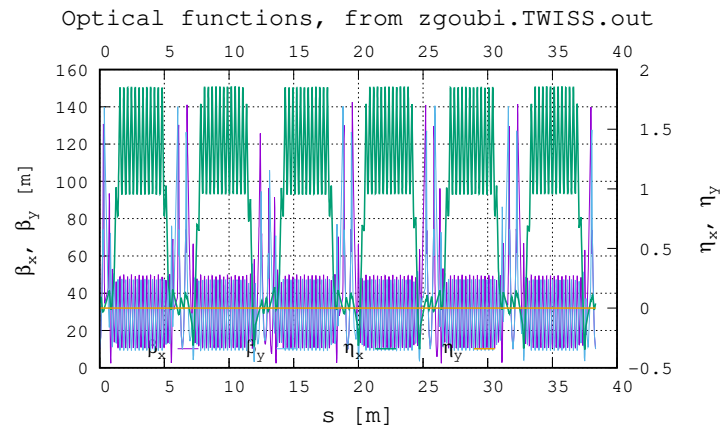


Figure 18: Optics with field maps, 300 A in coils 1 & 4. Fractional tunes  $\nu_Y = 0.69068/\nu_Z = 0.66596$ . Chromaticities re-tuned to  $\xi_Y = 1.9265/\xi_Z = 7.2696$ . IP6 and IP8  $\beta_{Y,Z}^* = 1.5$  m.

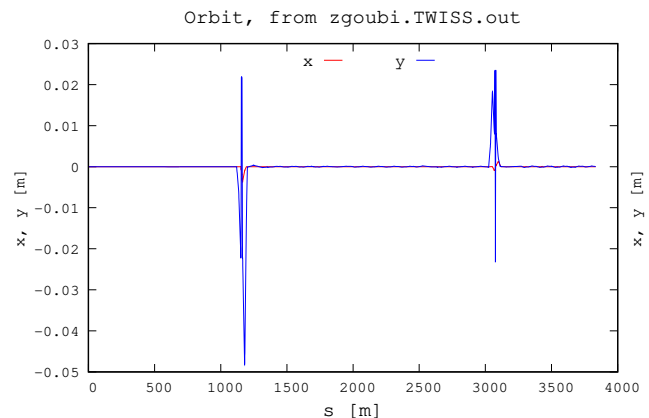


Figure 19: Orbits with local closed orbit bumps at snakes. IP separation bumps have been zero-ed.

Figures 20, 21 detail the  $\approx 90$  m extent local closed orbit bumps in 9 o'clock and 3 o'clock snake regions. Note the strong vertical orbit kick downstream of 9 o'clock, due to large orbit off-centering in B19\_QF7 (located at  $s=1165.28$  m); this throws the orbit at  $-50$  mm which is not acceptable. This can only be compensated with a non-zero, positive, orbit incidence at snake entrance, which allows decreasing the overall vertical excursion below  $\approx 30$  mm, this is addressed using Run 22 optics, Sec. 4.2.2, see Fig. 63 p. 23.

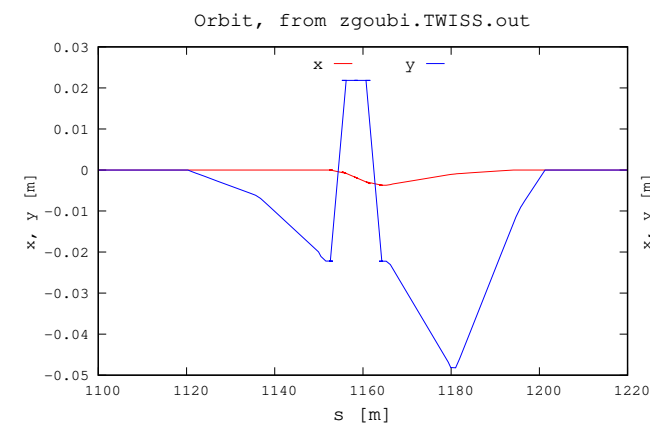


Figure 20: Closed orbit bump in 9 o'clock snake region (the 10.4 m snake extends around  $s \approx 1160$  m), case of 300 Amp in coils 1-4, an excerpt from Fig. 19. Note that the peak vertical excursion ( $-5$  cm) can be reduced (below 3 cm) by introducing a positive incidence of the orbit at entrance to the snake ( $s = 1151$  m)

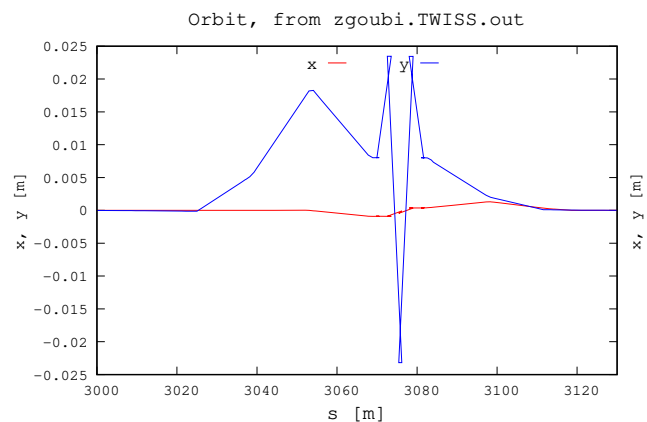


Figure 21: Closed orbit bump in 3 o'clock snake region (the 10.4 m snake extends around  $s \approx 3075$  m), case of 100/322 Amp, an excerpt from Fig. 19.

Figure 22 shows a transport of the spin closed orbit  $\vec{n}_o(s)$  around the ring.

As part of the search of an optimum setting, Figs. 23-24 detail the evolution of the 2-coil snake precession axis and spin precession by the snake, as a function of its coil current.

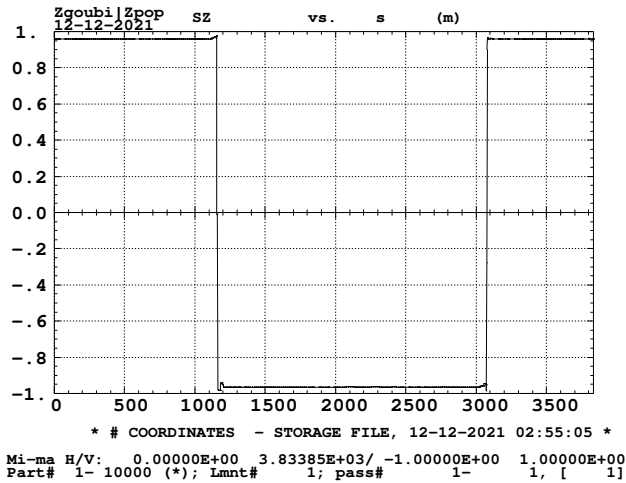


Figure 22: Vertical component of spin  $\vec{n}_0$  around RHIC Blue at  $G\gamma = 45.5$ . Coils 1&4 9 o'clock snake current 305 A, complete 3 o'clock snake 100/322 A.

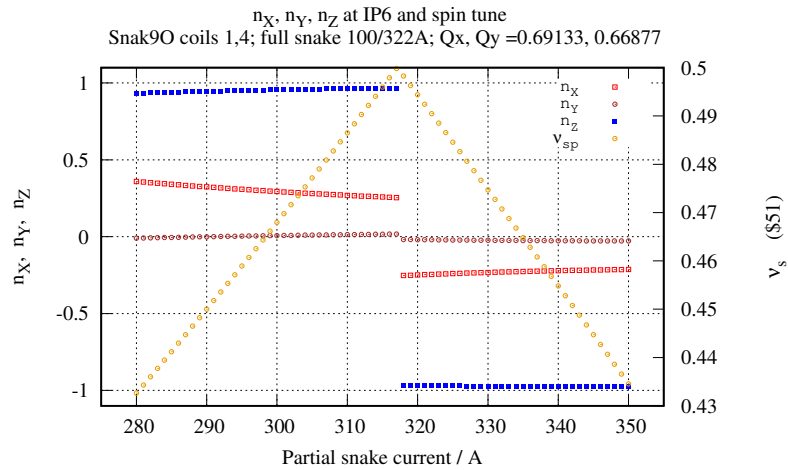


Figure 23: A scan of the components of RHIC Blue spin eigenvector  $\vec{n}_0(IP6)$ , and spin tune, versus current in coils 1 & 4 of 9 o'clock snake. Current is varied from 280 to 350 A. Higher current yields  $\vec{n}_0(IP6)$  closer to vertical

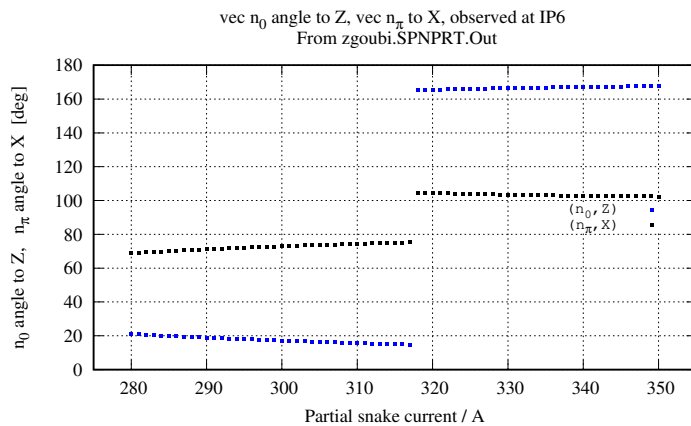


Figure 24: Angle of spin  $\vec{n}_0(IP6)$  to Z axis, and angle of projected  $\vec{n}_\pi(IP6) = (n_X, n_Y)$  to X axis, versus current in coils 1 & 4 of 9 o'clock snake.

### 3.1.2 At 255 GeV

With the previous injection settings, no further adjustment of snake currents, RHIC Blue 1-turn spin matrix out of this model at 255 GeV comes out to be

```

-0.878342    -0.259052    0.401755
 0.145023    -0.945228   -0.292426
 0.455503    -0.198585    0.867802

```

```

Determinant =      1.0000000000
Trace = -0.9557683760 ; spin precession = 167.9276244159 deg
Precession axis : ( 0.2243, -0.1285, 0.9660)
Spin tune Qs (fractional) :      4.6647E-01

```

which shows a 20 deg tilt of the spin precession axis at IP6 (rotators are off, here), and 0.466 spin tune. Simulation-wise, as a guidance regarding what is doable (or not) for RHIC operation, tweaking these quantities (via snake currents) allows getting  $\vec{n}_0$  closer to vertical and spin tune closer to 0.5, this is addressed in Sec. 3.1.3, pp. 15 on.

### 3.1.3 $\nu_{sp} = 393 + \nu_Z$ crossing

The goal of this simulation is to assess a possible depolarization upon traversal of the strongest snake resonance, during the acceleration to top energy, as a consequence of 9 o'clock snake being partial (160<sup>+</sup> deg, see Secs. 2.1, 2.2 and Figs. 24, 37).

A preliminary sanity check: the total deviation in bends around ring should be  $2\pi$ , this is confirmed:

```

-----
Found      132 arc bends, and      132 bends with KP=3 positioning.
Total deviation in these arc BENDs, ALE_tot = 5.1370400000000043 rad,      294.33071118988465 deg.
Found      72 other BENDs with KPOS=3, ALE_tot = 1.1460696140000002 rad,      65.664951910387373 deg
Total deviation = 6.2831096140000042 rad,      359.99566310027200 deg
-----

```

Crossing of the strong resonance  $\nu_{sp} = 393 + \nu_Z$  is displayed in Fig. 25: a single particle is launched on  $\epsilon_y = 2.5\pi\mu\text{m}$ , norm. RF voltage 3 MV. Initial spin is vertical. The 2-module 9 o'clock snake current is 300 Amp, 3 o'clock snake setting is nominal: -100/+322/-322/+100Amp. This result indicates absence of polarization loss through  $393 + \nu_Z$ . Figure 26 is for comparison: the snakes are simulated using pure precession (no snake field maps), results are qualitatively similar, with no clear evidence of depolarization.

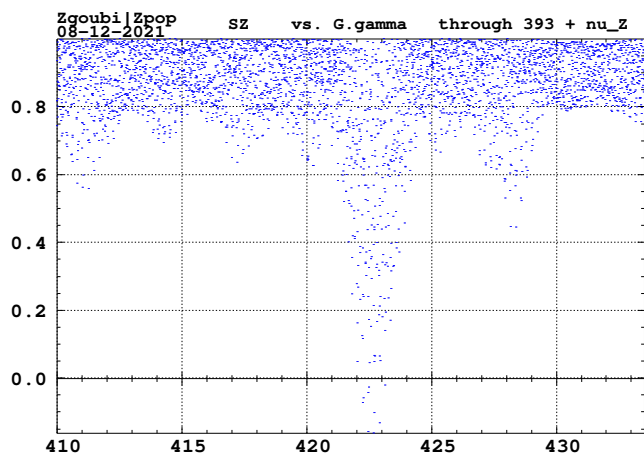


Figure 25: At IP6, tracking  $S_Z(G\gamma)$  across  $393 + \nu_Z$ , single particle on  $\epsilon_y = 2.5\pi\mu\text{m}$  normalized invariant. Spin starts vertical, obviously away from  $\vec{n}_0$ , however final oscillation of  $\vec{S}$  has similar amplitude, indicating absence of depolarization. See Figs. 26-30 for more

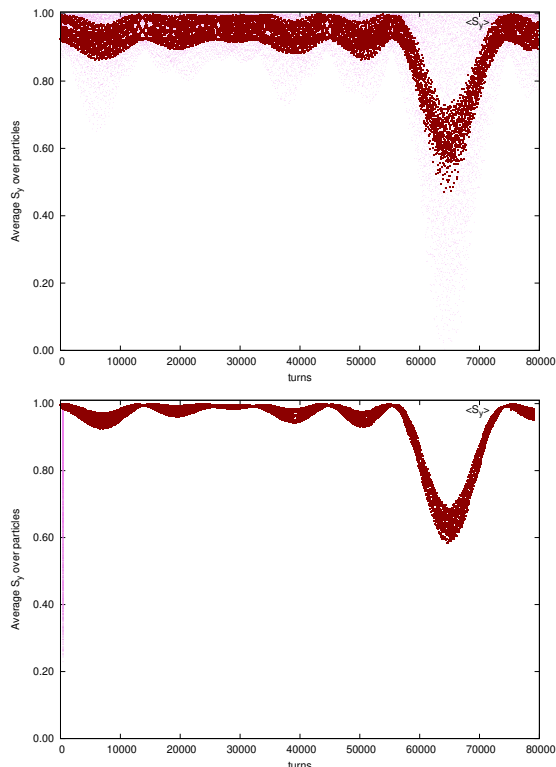


Figure 26: Crossing of  $393 + \nu_Z$ : case of pure rotation at both RHIC Blue snakes (no field maps used, no orbital effects): Top: case of 9 o'clock snake 88%; bottom: both snakes complete (4 coils), full-snakes. Red curve: turn-by-turn  $\langle S_Z \rangle$ , an average over the 3 particles tracked. Blue: the 3 individual motions.

Additional  $393 + \nu_Z$  crossing simulations, using various 9 o'clock snake currents, are shown in Figs. 27-30: 21 particles are launched with betatron phases evenly distributed on  $\epsilon_{yy} = 2.5 \pi \mu\text{m}$  normalized invariant. Initial spins are vertical. RF voltage 3 MV. The 2-module 9 o'clock snake current is 295, 300, 310 or 315 Amp, 3 o'clock snake setting is nominal:  $-100/+322/-322/+100$  Amp.

In conclusion, no obvious depolarization effect can be observed in either of these various 2-coil current cases. At the time of the study, quick feedback to RHIC operation regarding snake settings was required, thus these results were considered sufficient confirmation of the feasibility of operating RHIC blue with an incomplete, and partial ( $\approx 160^+$  deg), 9 o'clock snake, provided proper adjustment of both 9 o'clock and 3 o'clock snakes as detailed in Sec. 4.

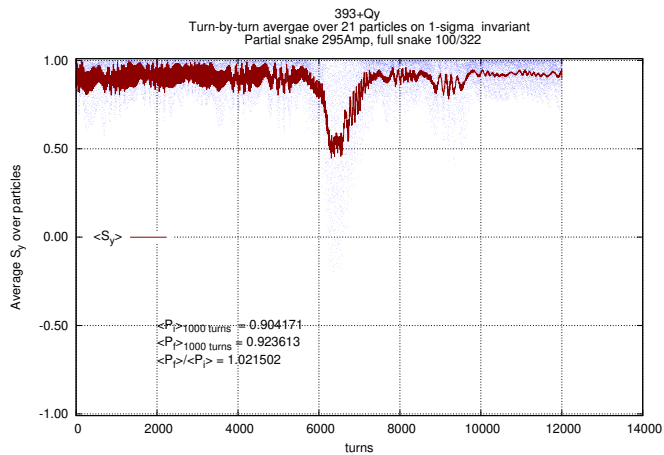


Figure 27: 9 o'clock snake current 295A.

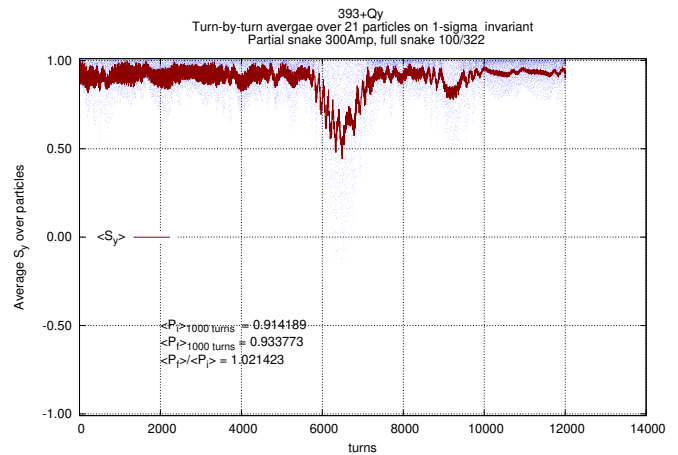


Figure 28: 9 o'clock snake current 300A.

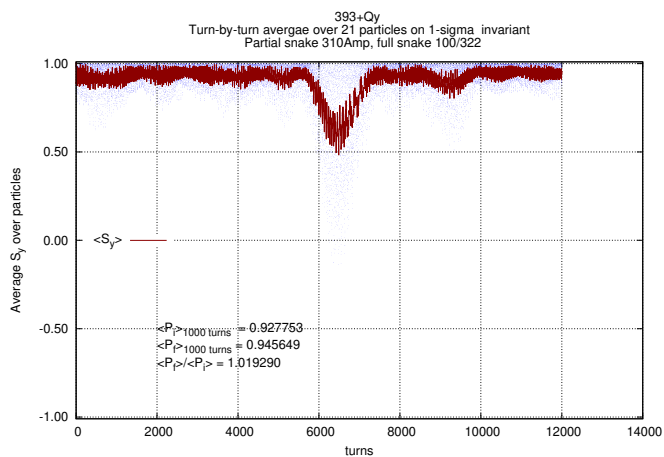


Figure 29: 9 o'clock snake current 310A.

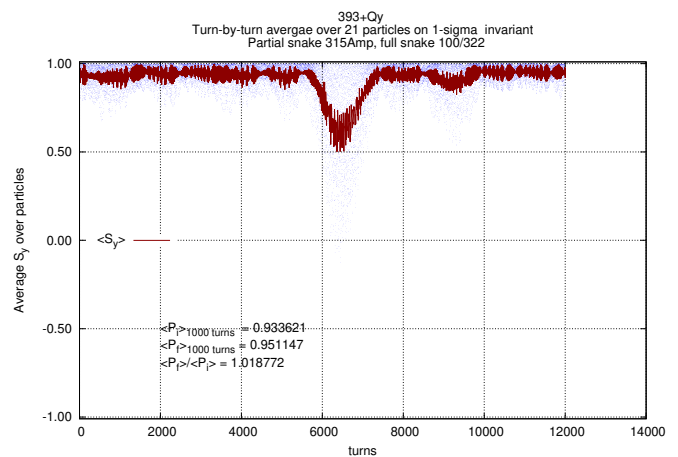


Figure 30: 9 o'clock snake current 315A.

### 3.2 Case of 1&3 coils 9 o'clock snake

No other possibility was left than operating RHIC Blue 9 o'clock snake with the remaining coils 1 and 3, after the loss of coil 4 (on Dec. 12, following from a power dip).

The same simulations as in Sec. 3.1 are repeated here, with the difference that coils 1&3 in 9 o'clock snake are used.

RHIC optics, closed orbit and local bumps are displayed in Figs. 31-34. Vertical orbit excursion downstream of 9 o'clock snake is again very large (Fig. 33), with the present orbit geometry of zero incidence at entrance in the snake, as for the coil 1-4 case.

Stable spin precession direction results are similar, they are summarized in Figs. 35-37. See comments in Sec. 3.1 for details, they essentially still hold here.

#### 3.2.1 At injection ( $G\gamma = 45.5$ )

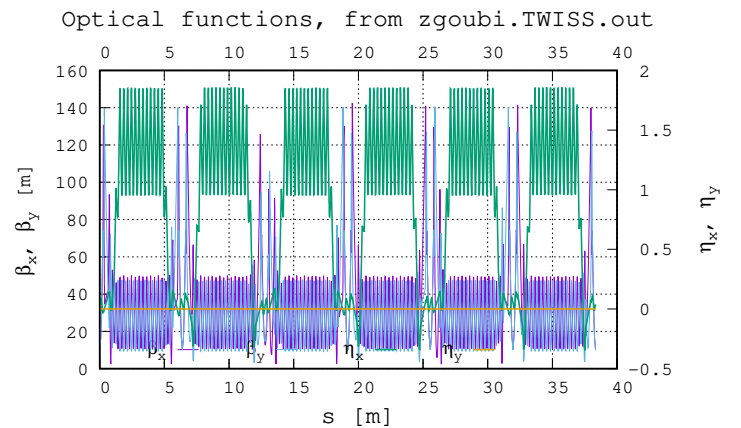


Figure 31: Optics at 320 A in coils 1 & 3. Fractional tunes  $\nu_Y = 0.69133/\nu_Z = 0.66877$ . Chromaticities  $\xi_Y = -12.759/\xi_Z = 3.42815$ . IP6 and IP8  $\beta_{Y,Z}^* = 1.5$  m.

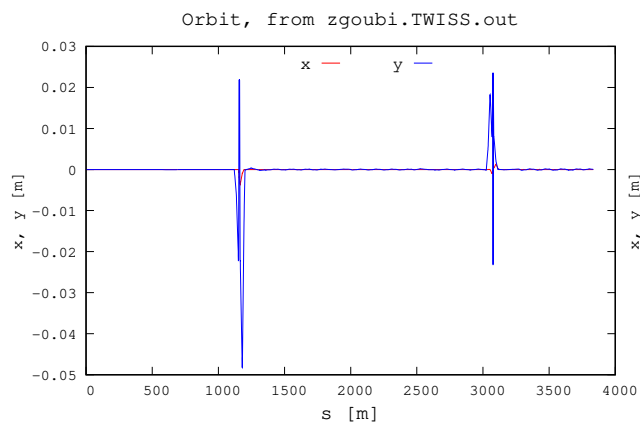


Figure 32: Orbits with snake bumps. IP bumps zero-ed.

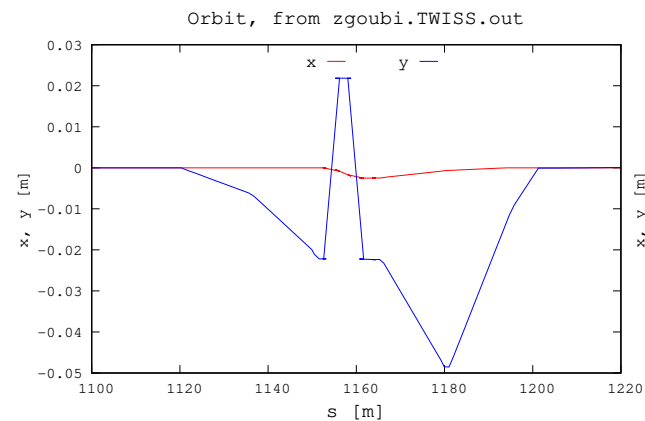


Figure 33: Orbit in 1&3 coil 9 o'clock snake 320 Amp, an excerpt from Fig. 32. Note that the peak vertical excursion (0.05 m) can be reduced (to  $\lesssim 3$  cm) provided a positive orbit incidence at snake entrance

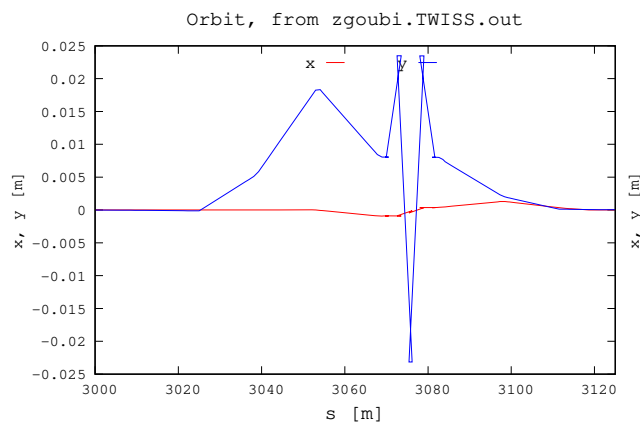


Figure 34: Orbit in complete 3 o'clock snake, 100/322 Amp coil currents, an excerpt from Fig. 32.

143 Computation of the 1-turn spin matrices show that 9 o'clock proper coils 1&3 currents (320 A about) allow near-vertical  $\vec{n}_0$ (IP6), and  
144 spin tune close to 0.5:

#### 1-turn spin matrix, coil current 300 A:

```

-0.807740    -0.187006    0.559093
 0.195840    -0.979615    -4.472663E-02
 0.556060     7.336507E-02    0.827898

```

```

Determinant = 1.0000000000
Trace = -0.9594576441 ; spin precession = 168.4438411422 deg
Precession axis : ( 0.2947, 0.0076, 0.9555)
Spin tune Qs (fractional) : 4.6790E-01

```

#### 1-turn spin matrix, coil current 320 A:

```

-0.875094    4.356607E-02    0.481989
-2.447622E-02 -0.998649    4.582732E-02
 0.483334    2.830593E-02    0.874978

```

```

Determinant = 1.0000000000
Trace = -0.9987649779 ; spin precession = 177.9863576138 deg
Precession axis : (-0.2493, -0.0191, -0.9682)
Spin tune Qs (fractional) : 4.9441E-01

```



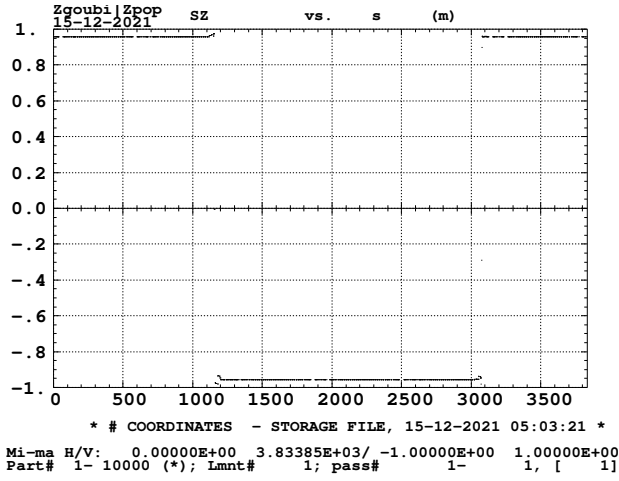


Figure 35: Typical vertical component of spin  $\vec{n}$  around RHIC at  $G\gamma = 45.5$ . Case of 320 A 1 & 3 coil 9 o'clock snake, and 100/322 A 3 o'clock snake.

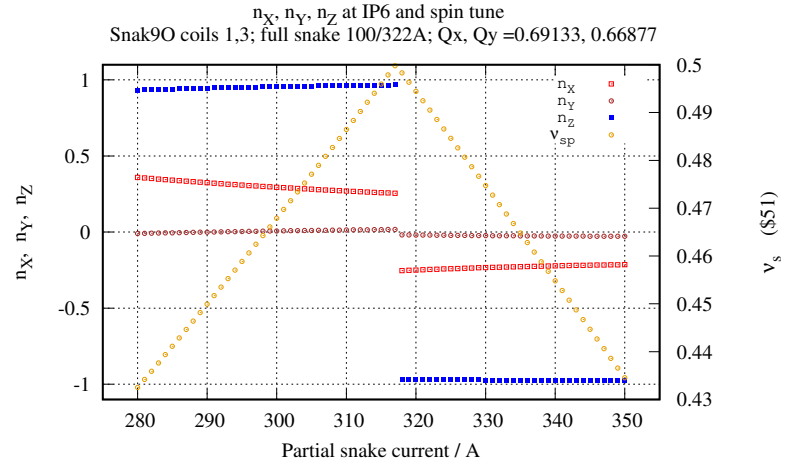


Figure 36: A scan of the components of RHIC Blue spin eigenvector  $\vec{n}_0(IP6)$ , and spin tune, versus current in coils 1 & 3 of 9 o'clock snake. Current is varied from 280 to 350 A. Higher current yields  $\vec{n}_0(IP6)$  closer to vertical

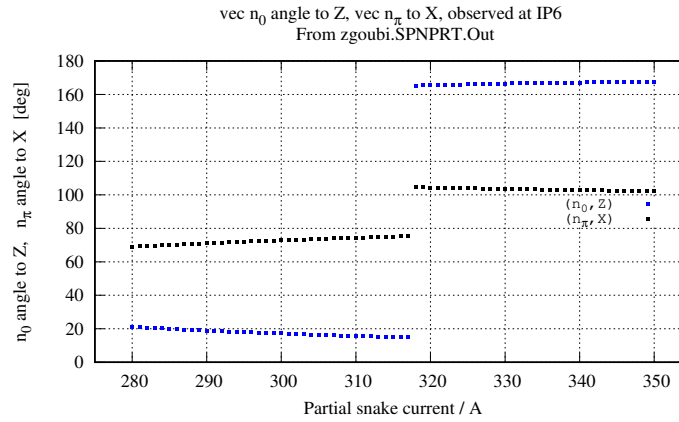


Figure 37: Angle of spin  $\vec{n}_0(IP6)$  to Z axis, and angle of projected  $\vec{n}_\pi(IP6) = (n_X, n_Y)$  to X axis, versus current in coils 1 & 3 of 9 o'clock snake.

### 147 9 o'clock and 3 o'clock snake settings for $n_Z(IP6)$ near 1 and $\nu_{sp}$ near 0.5

148 A fitting procedure is used to get  $n_Z$  closest to 1 at IP6 and  $\nu_{sp}$  closest to 1/2. Three variables are available: 9 o'clock snake 1&3 coil current,  
149 and 3 o'clock I1 (low field coils) and I2 (high field coils) currents, however two might be enough given that there is two constraints:  $n_Z$  and  
150 spin tune  $\nu_{sp}$ .

151 Note that in these hypotheses  $n_X$  and  $n_Y$  are ignored, which simulation-wise is justified as, *in fine*, it appears to be possible to bring  $n_z$   
152 very close to 1; such would not be the case if  $\vec{n}_0$  tilt from vertical was large, resulting in large  $\sqrt{n_X^2 + n_Y^2}$ , in that case the orientation of the  
153 projected  $\vec{n}_\pi = (n_X, n_Y)$  vector at STAR experiment at IP6 does matter.

154 Three different fitting results are given as an illustration in the following, however actual settings for Run 22 will be derived in Sec. 4.

155 Starting conditions are as in Sec. 3.2.1, namely 9 o'clock current 300A, 3 o'clock at 100/322, resulting in typical closed orbit of Fig. 38  
156 and projected helical trajectories of Figs. 39, 40, whereas  $n_Z = 0.9555$  and spin tune  $\nu_{sp} = 0.4679$ .

### Typical initial RHIC Blue optical conditions, prior to fitting

◇ For these fitting trials, periodic beam matrix at IP6, tunes and chromaticities are as follows:

```
Beam matrix (beta/-alpha/-alpha/gamma) and periodic dispersion
1.447635 -0.047603 0.000000 0.000000 0.000000 0.005250
-0.047603 0.692347 0.000000 0.000000 0.000000 0.006329
0.000000 0.000000 1.538271 -0.383621 0.000000 0.014793
0.000000 0.000000 -0.383621 0.745750 0.000000 -0.003302
```

```
          Betatron tunes (Q1 Q2 modes)
NU_Y = 0.70137907          NU_Z = 0.67260717
```

```
Chromaticities :
dNu_y / dp/p = -0.48883858          dNu_z / dp/p = 8.5068074
```

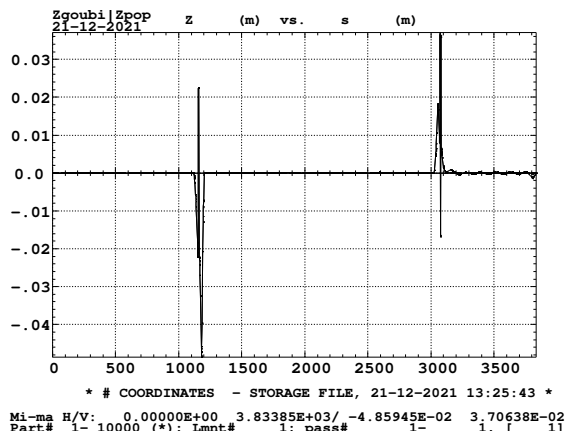


Figure 38: Typical vertical closed orbit around RHIC Blue, prior to fitting

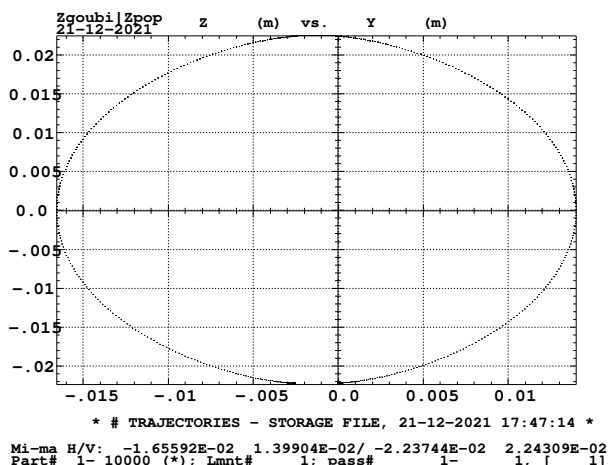


Figure 39: Helical orbit in partial 9 o'clock snake prior to fitting

◇ Initial field map scaling coefficient, prior to fitting:

```
TOSCA      snk1*
-1
1.         ! fit variable #36
1
TOSCA      snk2LowB
-1
1.         ! fit variable #40
1
TOSCA      snk2HighB
-1
1.         ! fit variable #44
1
```

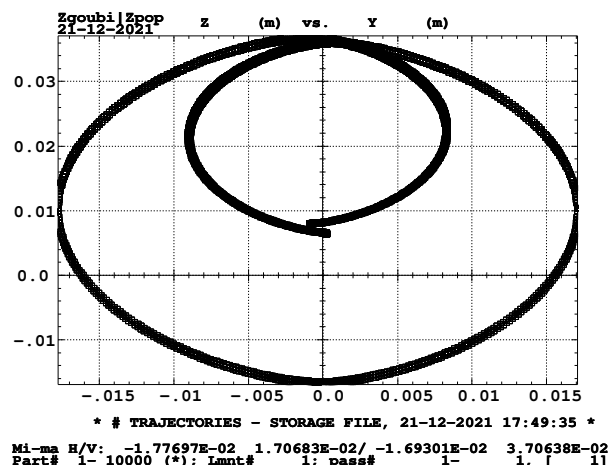


Figure 40: Double helix orbit in 3 o'clock snake prior to fitting

◇ FIT parameters, case of 3 variables as an example:

```
'FIT2'
3
6 36 0 .9 ! 9'O current
6 40 0 .9 ! 3'O low B
6 44 0 .9 ! 3'O high B
2 1e-10
10.3 1 3 #End 1. 1. 1 1 ! mom. group #, n_Z
10.4 1 1 #End .5 1. 0 ! mom. group 1, spin tune
```

• Using 2 variables: 9 o'clock snake and 3 o'clock high field coil current

This fit yields SCALING factor values

1.0816726/325 A in 9 o'clock snake, 0.98219937/316 A in 3 o'clock snake,

and

$$n_Z = 0.9749945, \quad \text{spin tune} = 0.4947627$$

◇ Resulting 1-turn spin matrix:

Spin transfer matrix, momentum group # 1 :

-0.900743	3.037657E-02	0.433288
-3.377972E-02	-0.999429	-1.560709E-04
0.433036	-1.477693E-02	0.901255

Determinant = 1.000000000  
 Trace = -0.9989172413; spin precession = 178.1145801993 deg  
 Precession axis : (-0.2222, 0.0038, -0.9750)

◇ Fitting outcomes:

STATUS OF VARIABLES (Iteration # 0 / 999 max.)										
LMNT	VAR	PARAM	MINIMUM	INITIAL	FINAL	MAXIMUM	STEP	NAME	LBL1	
6	1	36	0.108	1.08	1.0817660	2.06	3.222E-10	SCALING	-	
6	2	44	9.822E-02	0.982	0.98211781	1.87	4.475E-09	SCALING	-	

STATUS OF CONSTRAINTS (Target penalty = 1.0000E-10)										
TYPE	I	J	LMNT#	DESIRED	WEIGHT	REACHED	KI2	NAME	LBL1	
10	1	3	3001	1.000000E+00	1.000E+00	9.749945E-01		9.58E-01	OPTIONS	-
10	1	1	3001	5.000000E-01	1.000E+00	4.947627E-01		4.20E-02	OPTIONS	-

Fit reached penalty value 6.5270E-04

**Orbit monitoring** - As aforementioned, changing snake settings introduces some closed orbit (compare present Fig. 41 and the initial orbit condition prior to fitting Fig. 38), this is ignored as it is of little effect on periodic spin orbit and spin tune.

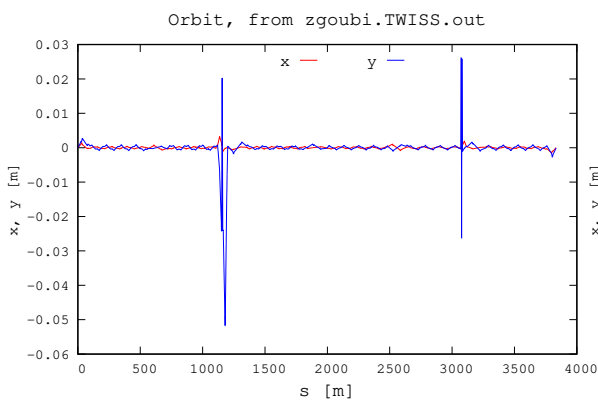


Figure 41: H and V closed orbits

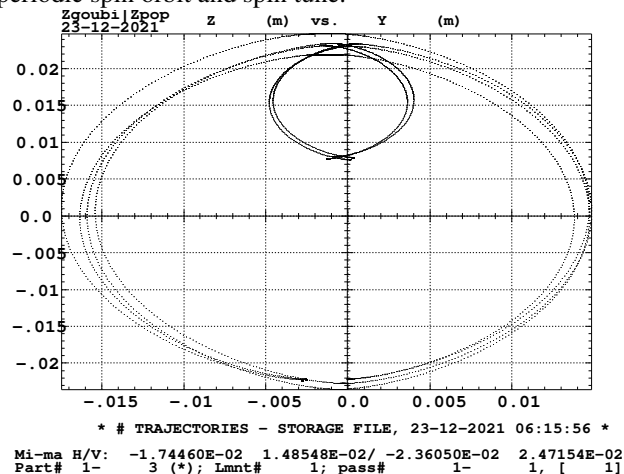


Figure 42: Sample projected helix, across each of the two snakes, changing during the fitting

• Using 2 variables: 9 o'clock snake and 3 o'clock low field coil current

3 o'clock high B coils current is 322A, frozen. In the tables below: 9 o'clock snake is the fit variable #36, 3 o'clock low B is variable #40.

```
'FIT2'
2
6 36 0 .9 ! 9'O current !
6 40 0 .9 ! 3'O low B ! 6 44 0 .9 ! 3'O high B
2 1e-10
10.3 1 3 #End 1. 1. 1 1 ! mom. group #, n_Z
10.4 1 1 #End .5 1. 0 ! mom. group 1, spin tune
```

STATUS OF VARIABLES (Iteration # 0 / 999 max.)										
LMNT	VAR	PARAM	MINIMUM	INITIAL	FINAL	MAXIMUM	STEP	NAME	LBL1	
6	1	36	0.109	1.09	1.0932648	2.08	8.552E-05	SCALING	-	
6	2	40	0.144	1.44	1.4376559	2.73	1.810E-04	SCALING	-	

STATUS OF CONSTRAINTS (Target penalty = 1.0000E-10)										
TYPE	I	J	LMNT#	DESIRED	WEIGHT	REACHED	KI2	NAME	LBL1	
10	1	3	3001	1.000000E+00	1.000E+00	9.998782E-01		1.00E+00	OPTIONS	-
10	1	1	3001	5.000000E-01	1.000E+00	4.999995E-01		1.92E-05	OPTIONS	-

Fit reached penalty value 1.4839E-08

This fit yields SCALING factor values

300 A\* 1.0932648 in 9 o'clock snake, 100 A\* 1.4750620 in 3 o'clock snake,

and

$$n_Z = 0.9998782, \quad \text{spin tune} = 0.4999995$$

Orbit monitoring:

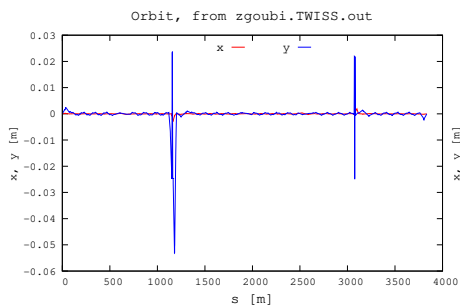


Figure 43: H and V RHIC orbits. The vertical excursion inside 9o'clock snake (at  $s \approx 1200$  m) is 24 mm, the 52 mm excursion observed here is outside, downstream of the snake, result of a simplistic bump closure.

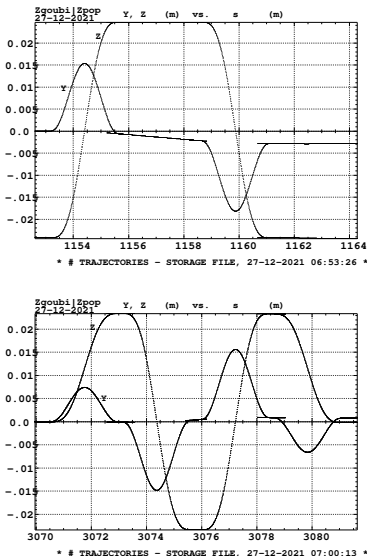


Figure 44: Closed orbits through the snakes, horizontal (Y) and vertical (Z).

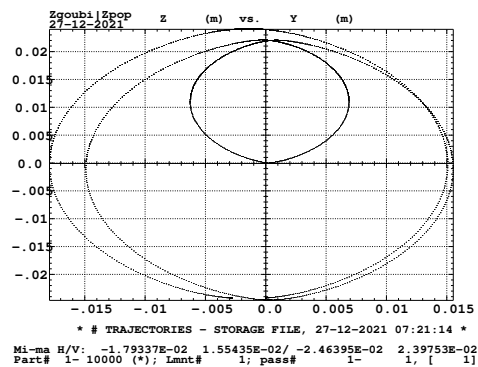


Figure 45: Projected helix, across each of the two snakes.

• Vary 3 o'clock low field only

Impose 9 o'clock current 322 A (the maximum acceptable) and leave 3 o'clock high B current 322 A:

```
'FIT2'
1 ! 6 36 0 .9 ! 9'O current !
6 40 0 .9 ! 3'O low B ! 6 44 0 .9 ! 3'O high B
2 1e-10
10.3 1 3 #End 1. 1. 1 1 ! mom. group #, n_Z
10.4 1 1 #End .5 1. 0 ! mom. group 1, spin tune

STATUS OF VARIABLES (Iteration # 0 / 999 max.) 3002
LMNT VAR PARAM MINIMUM INITIAL FINAL MAXIMUM STEP NAME LBL1
6 1 40 0.144 1.44 1.2993625 2.73 1.586E-04 SCALING -
STATUS OF CONSTRAINTS (Target penalty = 1.0000E-10)
TYPE I J LMNT# DESIRED WEIGHT REACHED K12 NAME LBL1
10 1 3 3001 1.000000E+00 1.000E+00 9.961040E-01 8.83E-01 OPTIONS -
10 1 1 3001 5.000000E-01 1.000E+00 4.985791E-01 1.17E-01 OPTIONS -
Fit reached penalty value 1.7198E-05
```

The matching procedure ends up with reasonable values

$$n_Z = 0.996104, \quad \text{spin tune} = 0.498579$$

and

$$100 \text{ A} * 1.2993625 = 130 \text{ Amp low-field 3 o'clock snake,}$$

### 3.2.2 At 255 GeV

This Section checks orbit and spin outcomes at 255 GeV, for the previous, injection energy, 300 A or 320 A 9 o'clock snake current cases. Currents in 3 o'clock snake are the usual 100/322A.

#### Current in coil 1&3 9 o'clock snake is 300 A

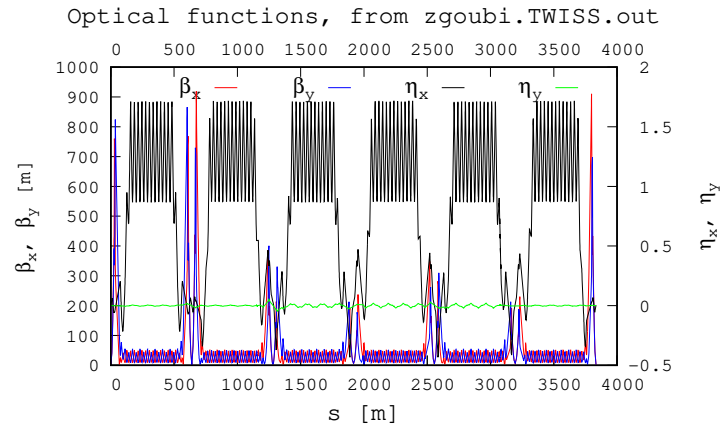


Figure 46: Optics. Fractional tunes  $\nu_Y = 0.70054329$ ,  $\nu_Z = 0.61854387$ . Chromaticities are +5/+4. IP6  $\beta_{Y,Z}^* = 1.49/1.63$  m.

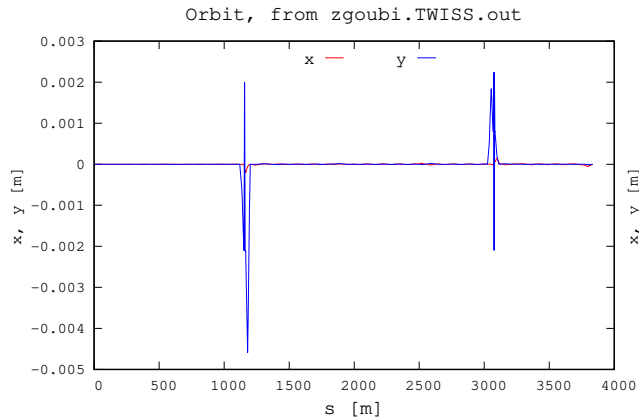


Figure 47: Orbits with snake bumps. IP bumps zero-ed.

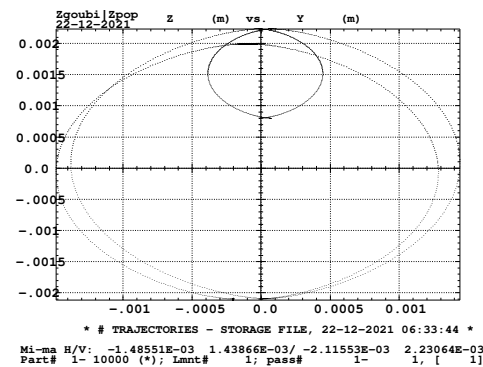


Figure 48: Projected helix, across each of the two snakes.

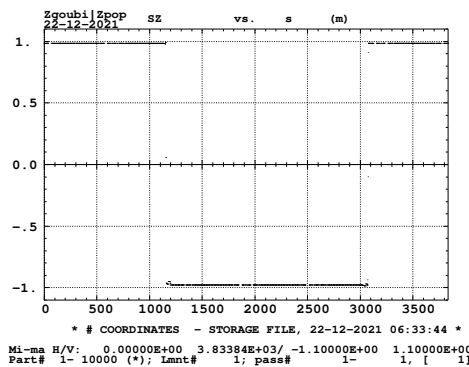


Figure 49: Vertical component of spin eigenvector around RHIC Blue

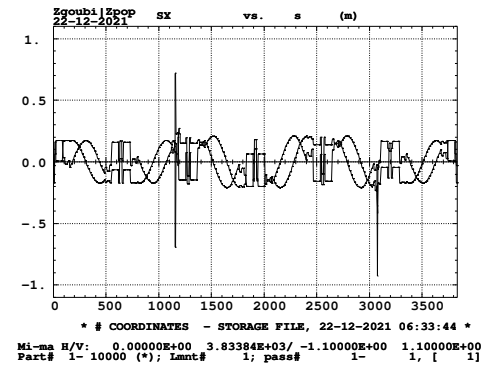


Figure 50: Horizontal components of spin eigenvector around RHIC Blue

#### 1-turn spin matrix, 255 GeV:

Spin transfer matrix, momentum group # 1 :

-0.966225	-0.236843	-0.101566
0.257179	-0.911297	-0.321554
-1.639928E-02	-0.336813	0.941428

Determinant = 1.0000000000  
Trace = -0.9360936967; spin precession = 165.476953 deg  
Precession axis : (-0.0304, -0.1698, 0.9850)  
Spin precession/2pi (or Qs, fractional) : 4.5966E-01

From the spin matrix:

- spin  $\vec{n}$  tilt to vertical: 9.936 deg;

- angle of  $\vec{n}_\pi = (n_X, n_Y)$  to X axis (long.) =  $\arctan \frac{n_Y}{n_X} = \arctan \frac{0.1698}{0.0304} = 79.849$  deg.

#### Spin eigenvector components at IP6 vs. energy

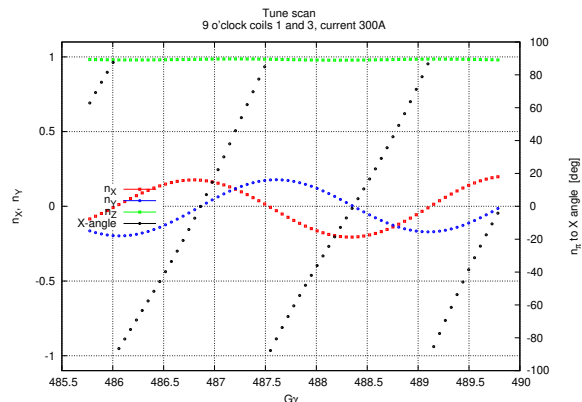


Figure 51: A scan of spin eigenvector components vs. energy, around RHIC Blue, 255 GeV

Current in coil 1&3 9 o'clock snake is 320 A

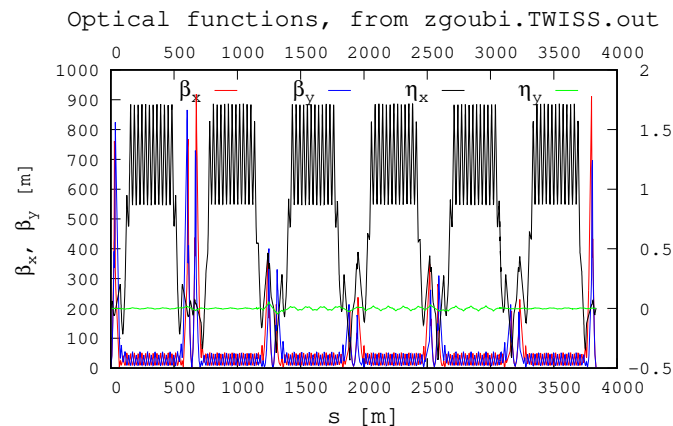


Figure 52: Optics. Fractional tunes  $\nu_Y = 0.70053934$ ,  $\nu_Z = 0.61857060$ . Chromaticities are +5/+4. IP6  $\beta_{Y,Z}^* = 1.49/1.63$  m.

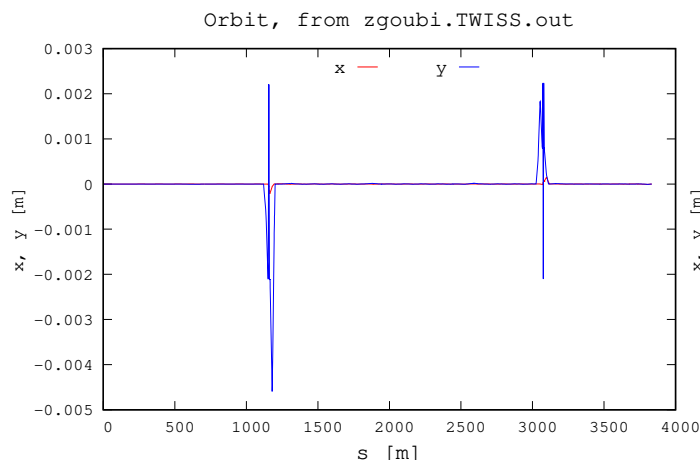


Figure 53: Orbits with snake bumps. IP bumps zero-ed.

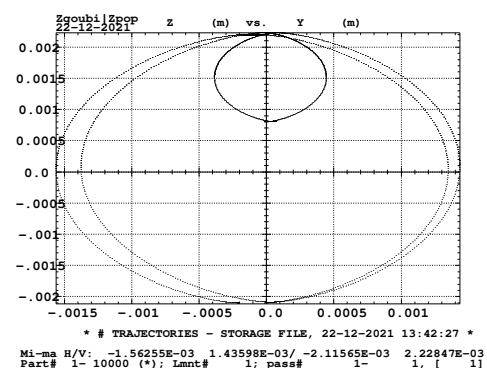


Figure 54: Projected helix, across each of the two snakes.

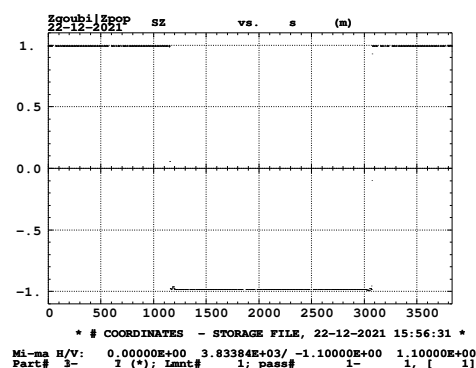


Figure 55: Vertical component of spin eigenvector around RHIC Blue

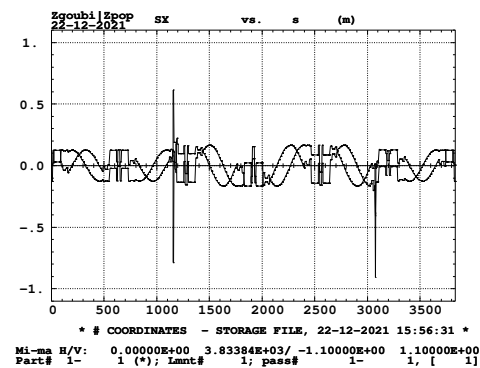


Figure 56: horizontal components of spin eigenvector around RHIC Blue

Spin eigenvector components at IP6 vs. energy

1-turn spin matrix, 255 GeV:

Spin transfer matrix, momentum group # 1 :

-0.999755	-2.187160E-02	3.337572E-03
2.033238E-02	-0.967727	-0.251180
8.723480E-03	-0.251049	0.967935

Determinant = 1.0000000000  
Trace = -0.9995477448; spin precession = 178.7815081945 deg  
Precession axis : ( 0.0031, -0.1266, 0.9920)  
Spin precession/2pi (or Qs, fractional) : 4.9662E-01

From the spin matrix:

- spin  $\vec{n}$  tilt to vertical: 9.936 deg;

- angle of  $\vec{n}_\pi = (n_X, n_Y)$  to X axis (long.) =  $\arctan \frac{n_Y}{n_X} = \arctan \frac{-0.1266}{0.0031} = -88.60$  deg.

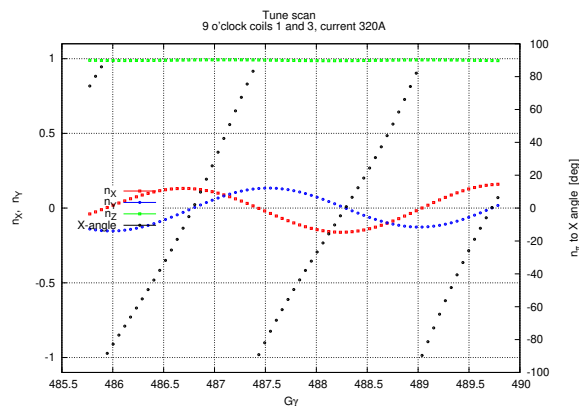


Figure 57: A scan of spin eigenvector components vs. energy, around RHIC Blue, 255 GeV

## 4 Polarization in RHIC Blue, using Run 22 optics

Mostly, earlier simulations are re-done using RHIC Blue Run 22 optics, translated from the MADX files used to model RHIC operation.

In conclusion: these simulations are consistent with the earlier results, for instance regarding nominal 9 o'clock and 3 o'clock snakes settings, respectively 322 A and 130/322 A.

### 4.1 Snake spin matrices

**9 o'clock snake, case of coils 1&3, -322/+322 A, spin matrix:**

$$G\gamma = 45.5$$

Spin transfer matrix, momentum group # 3 :

```
-0.187104    -0.959915    0.208696
-0.959952    0.223764    0.168588
-0.208529    -0.168795    -0.963340
```

```
Determinant = 1.0000000000
Trace = -0.9266800659; spin precession = 164.4378555494 deg
Precession axis : (-0.6288, 0.7776, -0.0001) at 129 deg to X-axis
Spin precession/2pi (or Qs, fractional) : 4.5677E-01
```

**3 o'clock snake, -130/+322/-322/+130A, spin matrix:**

$$G\gamma = 45.5$$

Spin transfer matrix, momentum group # 3 :

```
0.184654    0.966157    0.180121
0.966090    -0.144784    -0.213795
-0.180481    0.213491    -0.960129
```

```
Determinant = 1.0000000000
Trace = -0.9202587245; spin precession = 163.7662874059 deg
Precession axis : (0.7642, 0.6450, -0.0001) at 40 deg to X-axis
Spin precession/2pi (or Qs, fractional) : 4.5491E-01
```

$$G\gamma = 487$$

Spin transfer matrix, momentum group # 1 :

```
-0.177465    -0.960952    0.212315
-0.960997    0.215711    0.173068
-0.212109    -0.173320    -0.961754
```

```
Determinant = 1.0000000000
Trace = -0.9235070674; spin precession = 164.1025567575 deg
Precession axis : (-0.6323, 0.7747, -0.0001) at 129 deg to X-axis
Spin precession/2pi (or Qs, fractional) : 4.5584E-01
```

$$G\gamma = 487$$

Spin transfer matrix, momentum group # 1 :

```
0.192468    0.965082    0.177688
0.965050    -0.153333    -0.212525
-0.177859    0.212382    -0.960864
```

```
Determinant = 1.0000000000
Trace = -0.9217285579; spin precession = 163.9175969339 deg
Precession axis : (0.7669, 0.6417, -0.0001) at 40 deg to X-axis
Spin precession/2pi (or Qs, fractional) : 4.5533E-01
```

Importantly, these settings preserve  $129 - 40 \approx 90^\circ$  angle between the snake precession axes, so ensuring  $\nu_{sp} = 1/2$ .

Considering the expected vertical tilt from Eq. 4, with twice the defect as each snake contributes a similar amount, 16 deg about, the expected  $\bar{n}_0$  tilt from vertical is  $\delta/2 = 16^\circ$ , or 4% depolarization.

## 4.2 At injection ( $G\gamma = 45.5$ )

### 4.2.1 Injection optics

Current in 9 o'clock snake is 320 A (coils 1 & 3), currents in 3 o'clock snake are 130/322 A.

Figures 58, 59 show the optics from MADX, and from Zgoubi including snakes. The latter is obtained in the following way:

- RHIC optical sequence is translated from MADX;
- 9 o'clock and 3 o'clock 90 m snake segments, including snake field maps, are designed with local closed orbit bump: local H- and V-kickers at 9 o'clock and 3 o'clock are re-matched so to (i) have the helix centered in the snake, and to (ii) account for the rising IP separation bump which happens to overlap with the downstream end of the local vertical orbit bump at the snake, see Figs. 60, 61;
- 9 o'clock and 3 o'clock snake segments are then installed the ring.

While there, 9 o'clock closed orbit bump designs have been assessed where an incidence is given to the orbit at entrance of the snake, as this allows to reduce the orbit excursion, from  $\approx 5$  cm (Fig. 33, p. 14) down to 2.3 cm, Fig. 63.

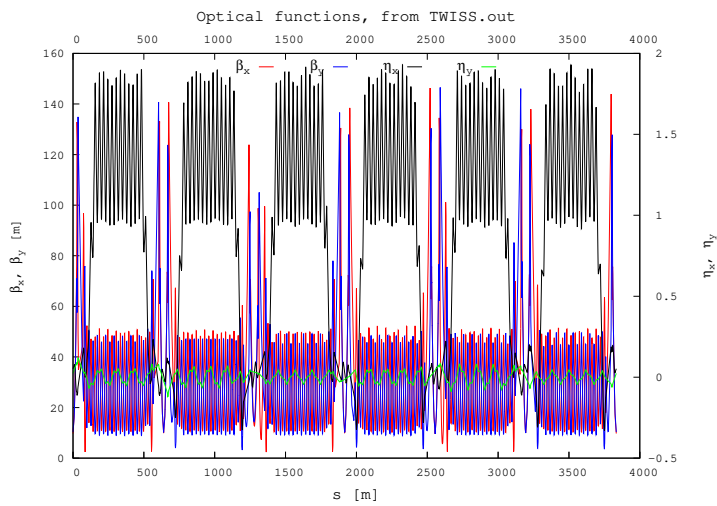


Figure 58: Blue optics at injection, from MADX model. Local bumps at snakes are set, but snakes are not included.

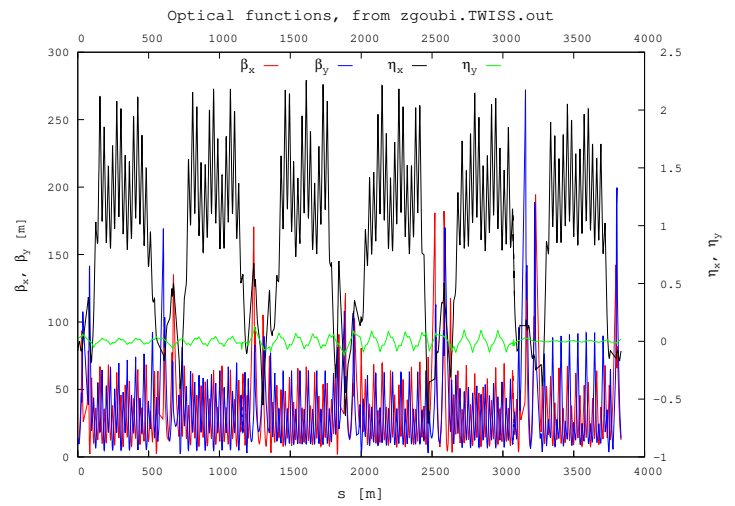


Figure 59: Blue optics at injection from Zgoubi model, brute from MADX translation and including snake OPERA field maps. Current in 9 o'clock snake is 320 A (coils 1 & 3), currents in 3 o'clock snake are 130/322 A.



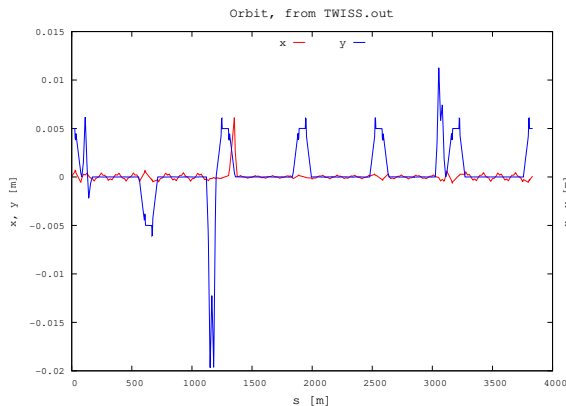


Figure 60: Closed orbits with snake bumps, from MADX.

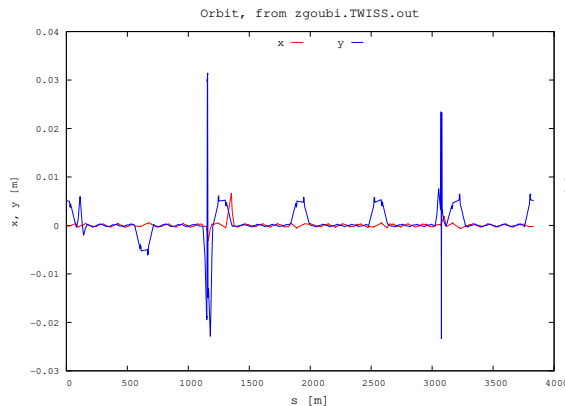


Figure 61: Closed orbits with snake field maps, from Zgoubi.

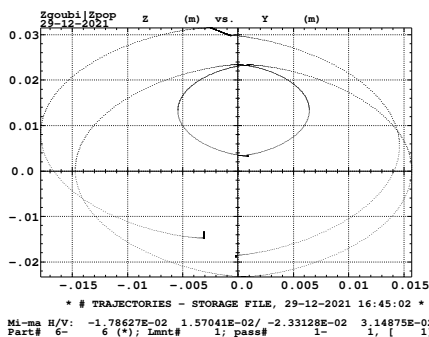


Figure 62: Y-Z projection of helical orbits in 9 o'clock/322A and 3 o'clock/130A/322A snakes.

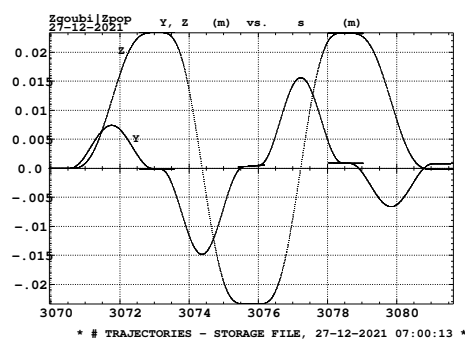
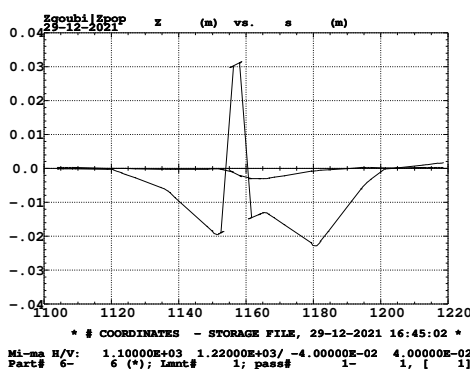


Figure 63: H and V closed orbit bumps at 9 o'clock and 3 o'clock snakes.

### 4.2.2 Spin, at injection

In the absence of rotators (spin essentially vertical all around), RHIC 1-turn spin matrix at  $G\gamma = 45.5$ , at IP6, is:

Spin transfer matrix, momentum group # 1 :

-0.992041	1.751470E-02	0.124688
-2.449474E-02	-0.998204	-5.466902E-02
0.123506	-5.728812E-02	0.990689

Determinant = 1.0000000000  
 Trace = -0.9995566888; spin precession = 178.7936176127 deg  
 Precession axis : (-0.0622, 0.0281, -0.9977)  
 Spin precession/2pi (or  $Q_s$ , fractional) : 4.9665E-01

yielding

$$n_z = \pm 0.9977 \text{ at IP6, spin tune} = 0.4966$$

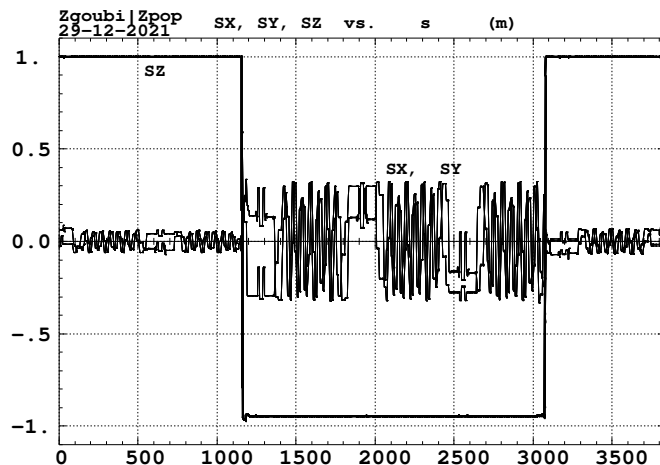


Figure 64: Components of the periodic spin vector around RHIC. Origin  $s=0$  is at IP6.

Table 2: Spin  $\vec{n}_0$  at clock 6, H-Jet and pC-polarimeter,  $G\gamma = 45.5$ .

s (m)	$S_x$ (long.)	$S_y$ (radial)	$S_z$ (vertical)	
0.	6.21418899E-02	-2.81117107E-02	9.97665624E-01	Clock6
1917.396	7.49266023E-02	3.13959328E-01	-9.46475327E-01	HJET
1988.033	1.22315357E-01	2.97096904E-01	-9.46980667E-01	pCPol

Transporting around the ring yields Tab. 2 and Fig. 64.

### 4.3 255 GeV optics ( $G\gamma = 487.253$ )

Current in 9 o'clock snake is 320 A (coils 1 & 3), currents in 3 o'clock snake are 130/322 A.

#### 4.3.1 255 GeV optics

Figures 65, 66 show the optics from MADX, and from Zgoubi including snake field maps. The latter is obtained in the following way:

- RHIC optical sequence is translated from MADX;
- 9 o'clock and 3 o'clock snake field maps are added.

By contrast with injection case (Sec. 4.2.1), there is no local correction of orbit bumps at snakes - the orbit defect they induce is marginal at such high rigidity.

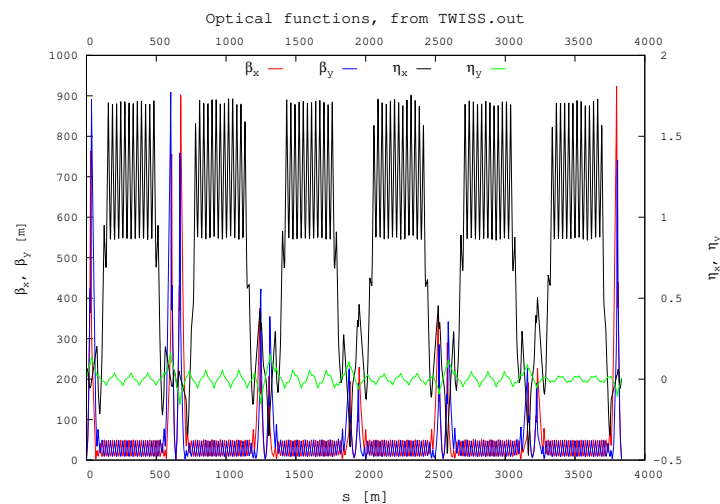


Figure 65: Blue optics at store energy, from MADX model.

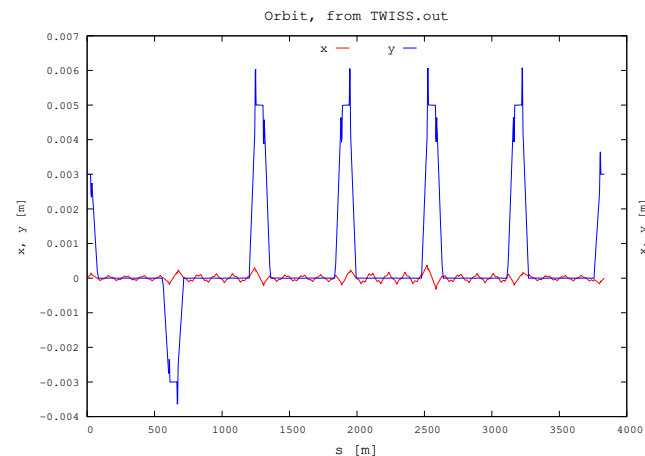


Figure 67: Closed orbits in MADX model. There is no orbit bump compensation at the snakes, at 255 GeV.

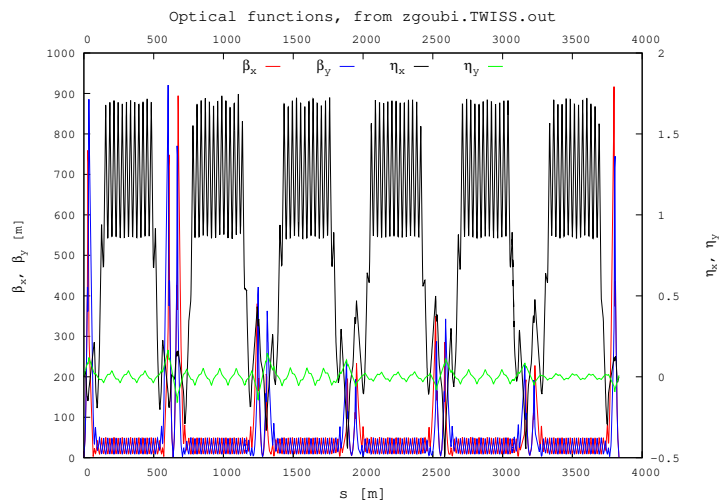


Figure 66: Blue optics at store energy, from Zgoubi model, which includes snake OPERA field maps. Current in 9 o'clock snake is 320 A (coils 1 & 3), currents in 3 o'clock snake are 130/322 A.

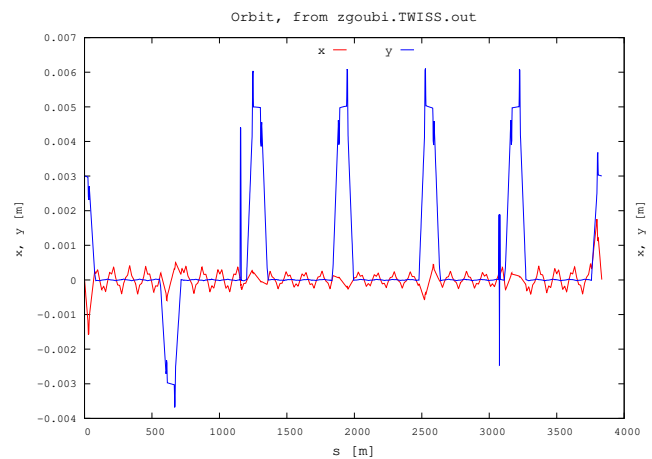


Figure 68: Closed orbits with snake field maps, from Zgoubi. The snake orbit defect is not compensated, hence a residual horizontal closed orbit.

### Orbits across the snakes, 255 GeV.

They are displayed in Figs. 69, 70. Incidentally, the  $\approx 0.2$  mm horizontal mis-centering of the helix in 3 o'clock snake seen in Fig.69, is mostly responsible for the residual (few 0.1 mm) horizontal periodic orbit around RHIC observed in Fig. 68.

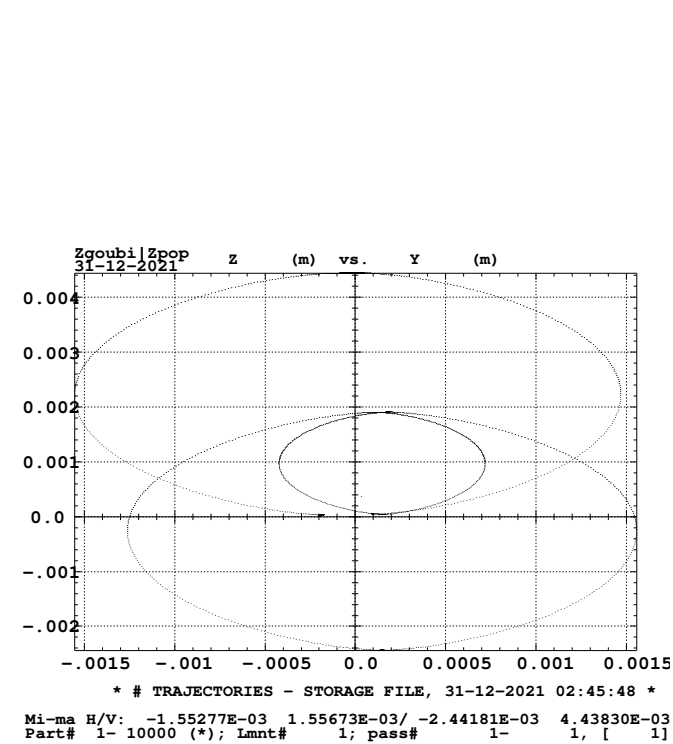


Figure 69: Y-Z projection of helical orbits in (upper one) 9 o'clock/322A and in (lower) 3 o'clock/130A/322A snakes. 255 GeV.

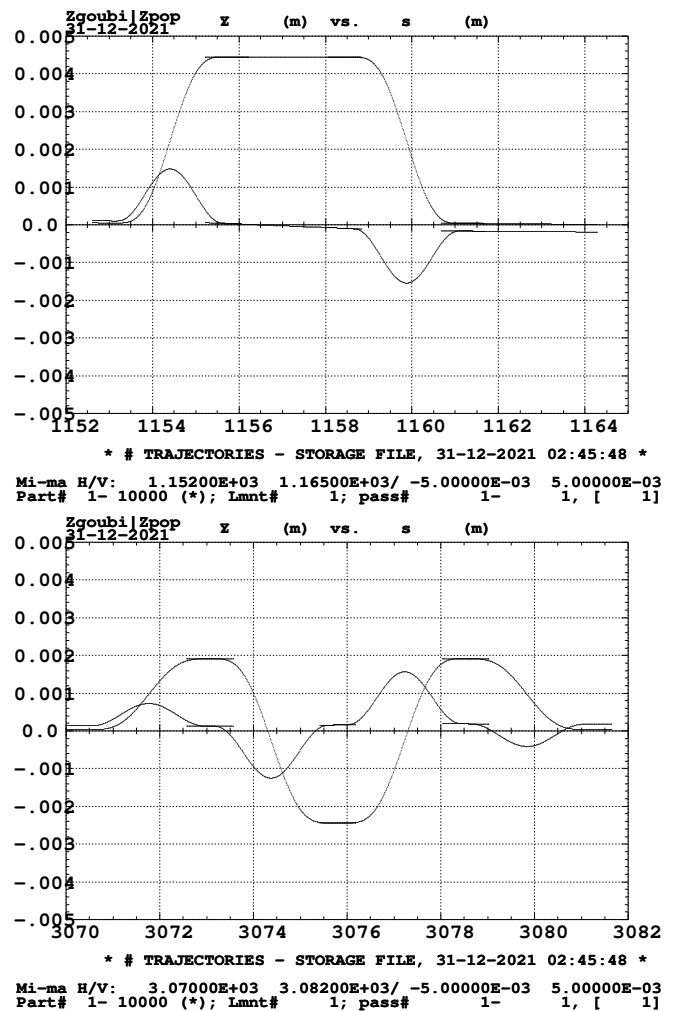


Figure 70: H and V bumps at 9 o'clock (top) and 3 o'clock (bottom) snakes. 255 GeV.

### 4.3.2 Spin, at 255 GeV

Details of spin motion along 9 o'clock and 3 o'clock snakes with these settings, namely, current in 9 o'clock snake 320 A (coils 1 & 3) and currents in 3 o'clock snake 130/322 A. are given in Figs. 71, 72.

RHIC 1-turn spin matrix at 255 GeV, at IP6, is

```
Spin transfer matrix, momentum group # 1 :
-0.963158      -5.240135E-02   0.263781
-5.087686E-02 -0.927620     -0.370045
 0.264080      -0.369832     0.890778

Determinant =      1.0000000000
Trace =      -0.9999993880;  spin precession =      179.9551780703 deg
Precession axis : ( 0.1357, -0.1902, 0.9723)
Spin precession/2pi (or Qs, fractional) :      4.9988E-01
```

yielding

$$n_Z = 0.9723 \text{ at IP6, } \text{spin tune} = 0.49988.$$

Transporting around the ring yields case  $G\gamma = 487.2532$  data in Tab. 2, and Fig. 73.

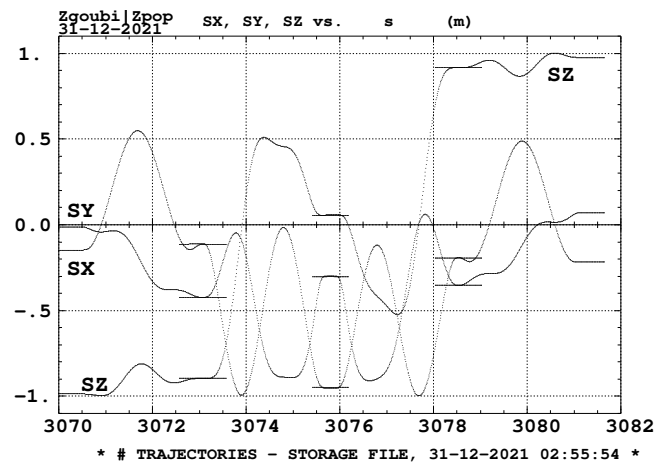
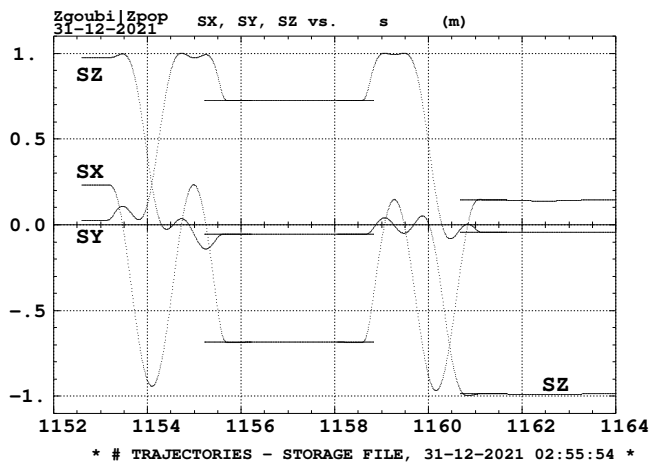


Figure 71: Spin  $\vec{n}_0$  components across 9 o'clock snake. 255 GeV.

Figure 72: Spin  $\vec{n}_0$  components across 3 o'clock snake. 255 GeV.

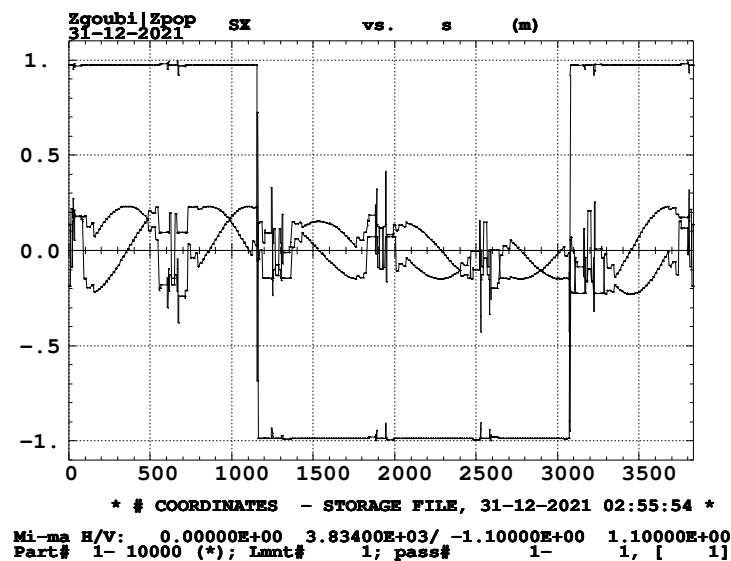


Figure 73: Spin  $\vec{n}_0$  components around RHIC Blue. 255 GeV.

215

Table 3 adds spin  $\vec{n}_0$  details at  $G\gamma = 485.74, 487, 487.25$  (as displayed in the following energy scans, Figs. 75-77).

Table 3: Spin  $\vec{n}_0$  at clock 6, H-Jet and pC-polarimeter,  $G\gamma = 485.7436$ .

s (m)	$n_X$ (long.)	$n_Y$ (radial)	$n_Z$ (vertical)	$\Phi = \text{atg} \frac{n_Y}{n_Z}$ [deg]	$\vec{n}_0$ to Z ang. [deg]	
0	8.14732E-03	6.22673E-02	9.98026E-01	3.57	3.60	STAR
1917.394	-6.73281E-03	-2.67909E-01	-9.63420E-01		164.46	HJET
1988.031	-3.09843E-01	5.99222E-02	-9.48897E-01	-3.61	161.60	pCpol_up
1988.539	-3.09843E-01	5.99222E-02	-9.48897E-01		161.60	pCpol_down

Table 4: Spin  $\vec{n}_0$  at clock 6, H-Jet and pC-polarimeter,  $G\gamma = 487.00$ .

s (m)	$n_X$ (long.)	$n_Y$ (radial)	$n_Z$ (vertical)	$\Phi = \text{atg} \frac{n_Y}{n_Z}$ [deg]	$\vec{n}_0$ to Z ang. [deg]	
0	1.31609E-01	-2.38564E-01	9.62167E-01	-13.93	15.81	STAR
1917.394	-2.91903E-02	4.56341E-02	-9.98531E-01		176.89	HJET
1988.031	-5.04563E-04	1.79328E-02	-9.99839E-01	-1.03	178.97	pCpol_up
1988.539	-5.04563E-04	1.79328E-02	-9.99839E-01		178.97	pCpol_down

Table 5: Spin  $\vec{n}_0$  at clock 6, H-Jet and pC-polarimeter,  $G\gamma = 487.2532$ .

s (m)	$n_X$ (long.)	$n_Y$ (radial)	$n_Z$ (vertical)	$\Phi = \text{atg} \frac{n_Y}{n_Z}$ [deg]	$\vec{n}_0$ to Z ang. [deg]	
0	1.35723E-01	-1.90235E-01	9.72311E-01	13.51		STAR
1917.394	-9.81521E-02	1.17065E-01	-9.88262E-01		171.21	HJET
1988.031	8.41464E-02	7.04441E-02	-9.93960E-01	-5.05	173.70	pCpol_up
1988.539	8.41464E-02	7.04441E-02	-9.93960E-01		173.70	pCpol_down

216

Some comments, referring to Tab. 3 and Figs. 75-77:

217

(i) simulations in this perfect RHIC Blue lattice seem consistent with measurements in the region  $G\gamma = 485.5 \sim 486$  (RHIC store 32920, 12/29/21, 16:56 on), namely:

219

@ STAR:

222

-  $n_Y$  (radial) component small ( $\approx 6 \times 10^{-2}$ );

223

- an off-vertical tilt, of the projection ( $n_{YZ}$ ) of 3-D spin  $\vec{n}_0$  into transverse (Y,Z) plane, of small value (3.6 deg at  $G\gamma = 485.75$ , see Fig. 75);

224

225

@ pC-pol: same result,

226

-  $n_Y$  (radial) component small ( $\approx 6 \times 10^{-2}$ );

227

- tilt wrt Z axis of 3-D spin projection in (Y,Z)-plane is small (-3.6 deg at  $G\gamma = 485.75$ , see Fig. 77);

228

229

(ii) On the other hand the simulation shows,

230

@ STAR: the 3-D stable spin precession vector  $\vec{n}_0$  is close to vertical, 3.6 deg tilt wrt Z at  $G\gamma = 485.75$  (Fig. 75),  $n_Z = 0.99802$  from simulation (Fig. 74);

232

233

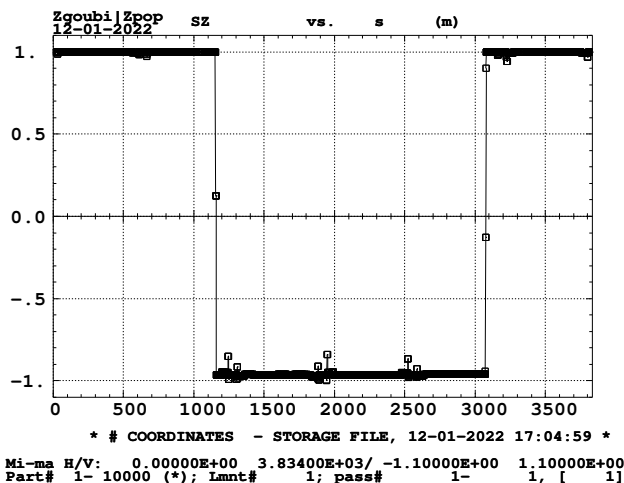


Figure 74: Vertical spin component  $n_Z$  around RHIC Blue, at  $G\gamma = 485.75$  (254.21 GeV/c).  $n_Z = 0.99802$  at STAR. Note: as expected,  $\vec{n}_0$  is seen to move away from vertical at IP separation bumps rise and fall

234  
235  
236  
237  
238  
239  
240  
241  
242  
243

@pC-pol: there is a substantial longitudinal component,  $n_X = -0.30984$ , the 3-D stable spin precession vector is tilted 18.4 deg from vertical (Z) axis at  $G\gamma = 485.75$ , its component  $n_Z = -0.948897$  (Fig. 74).

(iii) Results seem reversed at 255 GeV: STAR/pC-pol  $5^\circ/18^\circ$  measured, versus  $13.5^\circ / -5^\circ$  simulated ( $G\gamma = 487.25$ ).

4.3.3 Scans of  $\vec{n}_0$  components, at STAR, H-Jet, pC-Polarimeter

$G\gamma$  scans of  $\vec{n}_0$  components, at STAR, H-Jet, pC-Polarimeter, at 255 GeV, are displayed in Figs. 75-79. Two different techniques are used, for double-check mostly: numerical search of  $\vec{n}_0$  on the one hand (this uses a matching procedure, with constraint 1-turn periodic  $\vec{n}_0(s = 0)$ ), Figs. 75-77, and 1-turn spin matrix on the other hand, Figs. 78-79.

From numerical search of periodic  $\vec{n}_0$

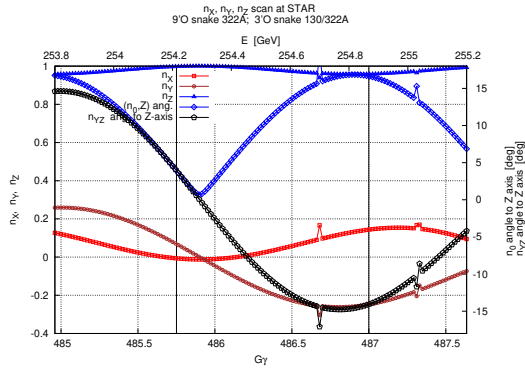


Figure 75: Spin  $\vec{n}_0$  components at STAR, and spin angle to Z (vertical) axis.  $\vec{n}_{YZ}$  denotes the projection of  $\vec{n}_0$  in the (Y,Z) plane.

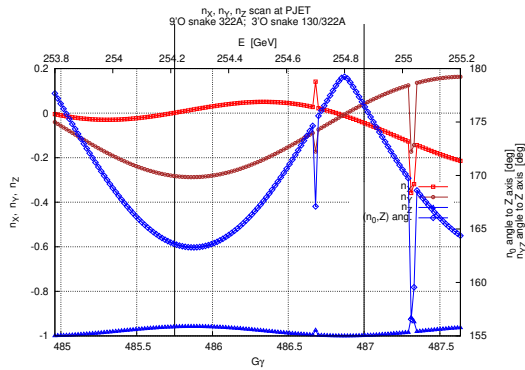


Figure 76: Spin  $\vec{n}_0$  components vs.  $G\gamma$  in 255 GeV region, at H-Jet.

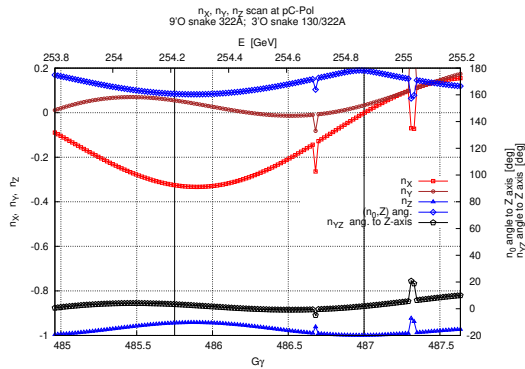


Figure 77: Spin  $\vec{n}_0$  components vs.  $G\gamma$  in 255 GeV region, at pC-polarimeter.  $\vec{n}_{YZ}$  denotes the projection of  $\vec{n}_0$  in the (Y,Z) plane.

From 1-turn spin matrix

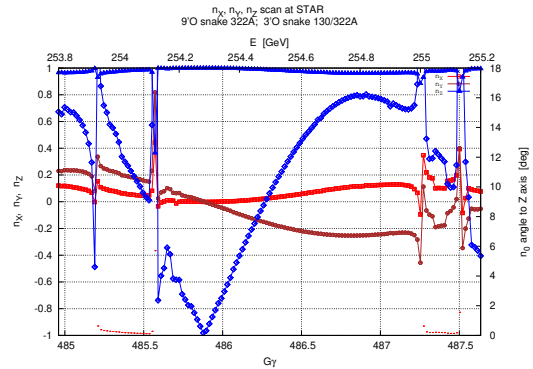


Figure 78: Spin  $\vec{n}_0$  components at STAR, and spin angle to Z (vertical) axis.

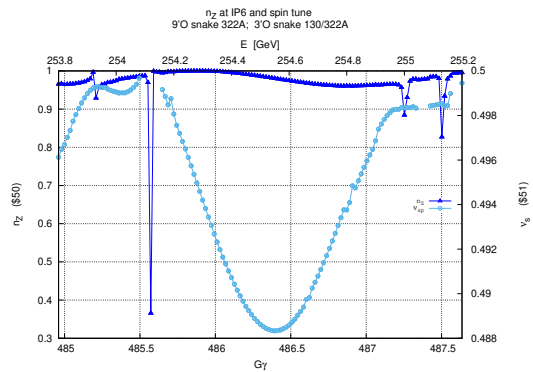


Figure 79: Spin  $n_Z$  component at STAR, and spin tune.

## 5 Polarization in RHIC Yellow with spin rotators, Run 22 optics

RHIC Yellow model in this Section is CW, translated from Run 22 CW MADX model. Zgoubi input files (and various “.res” execution listings) are available at

[https://sourceforge.net/p/zgoubi/code/HEAD/tree/trunk/exemples/RHIC/rotatorsWithFieldMaps/examples/RHIC\\_Yellow - CW\\_withSnakesAndRotators/](https://sourceforge.net/p/zgoubi/code/HEAD/tree/trunk/exemples/RHIC/rotatorsWithFieldMaps/examples/RHIC_Yellow - CW_withSnakesAndRotators/)

During Run 22, spin manipulations were performed using the IP6 spin rotators. This is the reason for the simulations discussed here. Section 6 details the way field maps of the rotators, which are comprised of both right- and left-helicity modules, were derived from the existing right-helicity snake field maps.

In a first step that clockwise Yellow model as set up for these studies is checked, at injection, Sec. 5.1, and at 255 GeV, Sec. 5.2; polarization properties are assessed in both cases. Spin rotators are added (Sec. 5.3) and used to tweak  $\vec{n}_0$  at IP6 (Sec. 5.4).

### 5.1 At injection ( $G\gamma = 45.5$ )

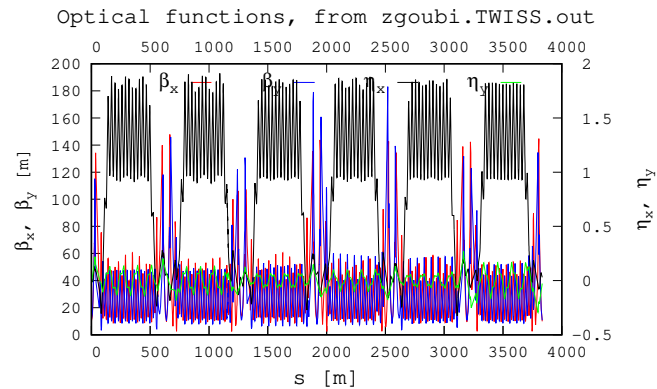


Figure 80: RHIC Yellow injection optics with snake field maps only. Coil currents 100/322 Amp. Fractional tunes  $\nu_Y = 0.7032/\nu_Z = 0.6837$ . Chromaticities  $\xi_Y \approx 2/\xi_Z \approx 11$ . IP6  $\beta_{Y,Z}^* = 10.0/9.9$  m.

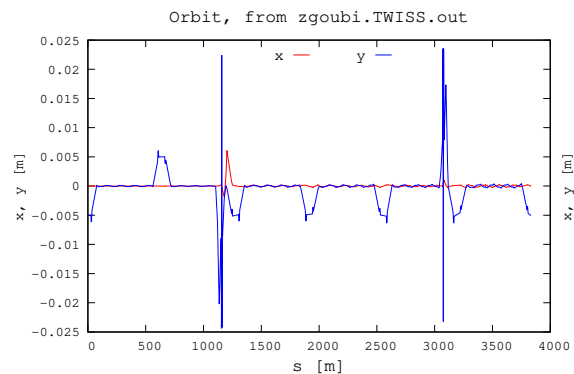


Figure 81: Orbits with snake bumps and IP separation bumps

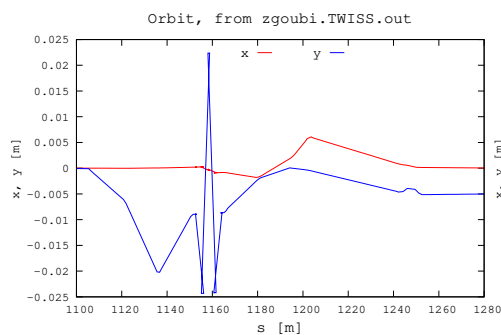


Figure 82: Orbit in 9 o'clock yellow snake and overlapping nascent vertical IP bump.

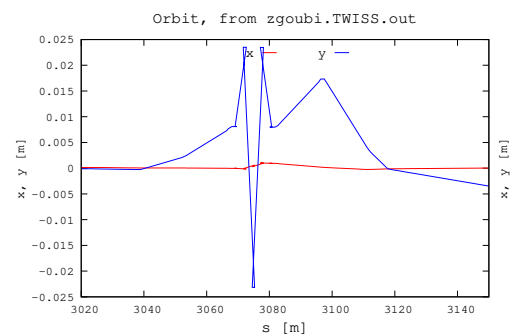


Figure 83: Orbit in 3 o'clock yellow snake and overlapping nascent vertical IP bump.

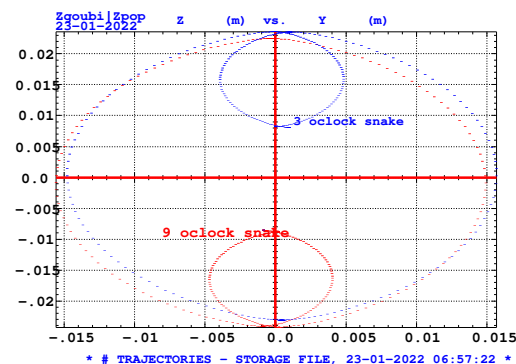


Figure 84: Transverse projection of helical trajectories in snakes, injection.

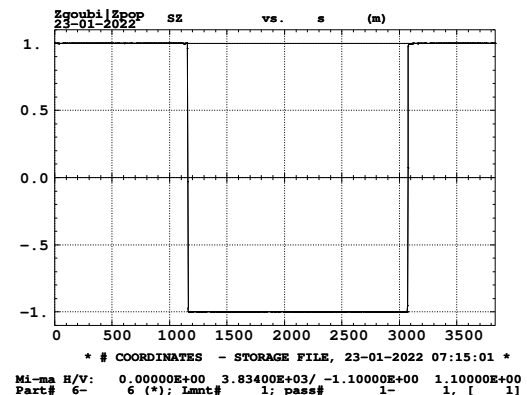


Figure 85: Spin  $\vec{n}_0$  around yellow, injection ( $G\gamma = 45.5$ ).

244 **Spin matrices at injection:**

• STAR to H-Jet

Spin transfer matrix, momentum group # 1 :

-0.385271	-0.922185	-3.377407E-02
-0.915548	0.386566	-0.111080
0.115492	-1.187411E-02	-0.993237

• STAR to PC-POL

Spin transfer matrix, momentum group # 1 :

-0.230165	-0.973091	-1.082156E-02
-0.966389	0.229860	-0.115137
0.114527	-1.604279E-02	-0.993291

• 1-turn spin matrix at IP6

Spin transfer matrix, momentum group # 1 :

-0.991209	-5.600912E-02	-0.119862
5.372817E-02	-0.998309	2.218013E-02
-0.120902	1.554518E-02	0.992543

Determinant = 1.0000000000  
 Trace = -0.9969758699; spin precession = 176.8487881094 deg  
 Precession axis : (-0.0603, 0.0095, 0.9981)  
 Spin precession/2pi (or Qs, fractional) : 4.9125E-01

$$n_Z = 0.9981 \text{ at IP6, } \nu_{sp} = 0.491$$

5.2 At 255.200 GeV,  $G\gamma = 487.635$

Optical functions, from zgoubi.TWISS.out

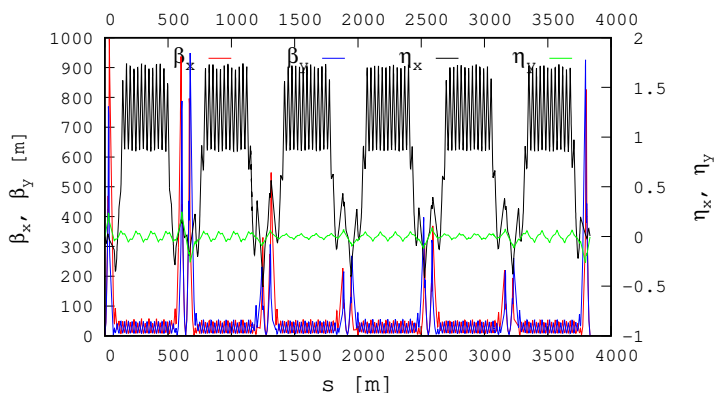


Figure 86: Optics with snake field maps only. Fractional tunes  $\nu_Y = 690795/\nu_Z = 0.685185$ . Chromaticities  $\xi_Y = 4.8/\xi_Z = 5.1$ . IP6  $\beta_{Y,Z}^* = 1.38, 1.46$  m.

Orbit, from zgoubi.TWISS.out

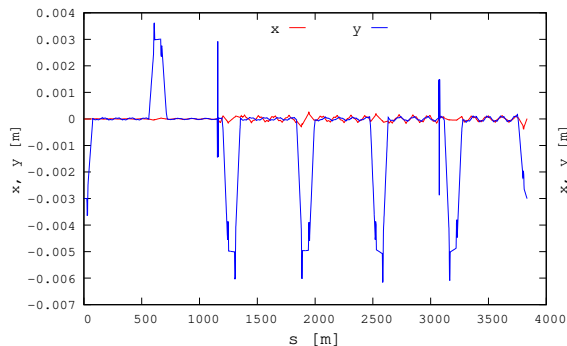


Figure 87: Orbits with snake bumps.

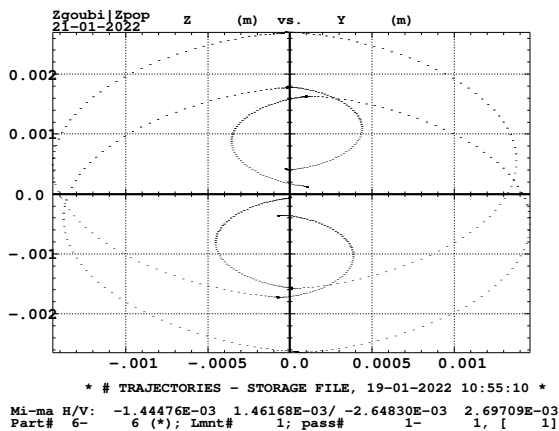


Figure 88: Transverse projection of helical trajectories in snakes.

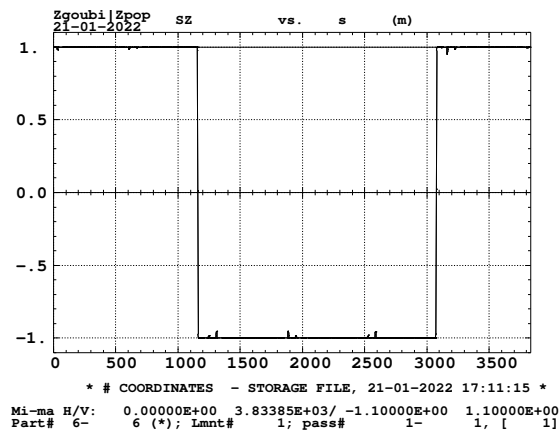


Figure 89: Spin  $\vec{n}_0$  around yellow, 255.200 GeV,  $G\gamma = 487.635$ .



248 **Spin matrices at 255.20 GeV:**

## • STAR to H-Jet

```

249      0.922957      0.383157      3.661774E-02
      0.383660      -0.923443      -7.585539E-03
      3.090795E-02      2.104989E-02      -0.999301

```

## • STAR to PC-POL

```

      -0.546299      0.835998      5.162566E-02
      0.837585      0.545042      3.714551E-02
      2.915401E-03      6.353344E-02      -0.997975

```

## 250 • 1-turn spin matrix at IP6

Spin transfer matrix, momentum group # 1 :

```

251      -0.993227      -0.108038      -4.276427E-02
      0.110139      -0.992644      -5.028051E-02
      -3.701749E-02      -5.464995E-02      0.997819

```

```

Determinant =      1.0000000000
Trace =      -0.9880510083; spin precession =      173.7337932103 deg
Precession axis : (-0.0200, -0.0263, 0.9995)
Spin precession/2pi (or Qs, fractional) :      4.8259E-01

```

252 **5.3 Add spin rotators**

253 A left-handed spin rotator is fabricated from a right-handed snake module (snakes are RRRR series with alternating sign, Fig. 3), this is  
 254 detailed in Sec. 6. This allows implementing a  $\begin{cases} \text{RLRL sequence if going CW} \\ \text{LRLR sequence if going CCW} \end{cases}$  (Fig. 3) in RHIC Yellow CW or CCW lattice model.

255 **Sanity check, first: move  $\vec{S}$  to longitudinal at STAR**

256 Spin rotators are introduced at STAR, store conditions are considered here, beam energy 255 GeV. They are set in this Section to move  
 257 spin  $\vec{n}_0$  to longitudinal at STAR.

258 The field along the closed orbit through the 6 o'clock rotator is displayed in Fig. 93. With peak fields  $B_{out} \approx 3.5$  T,  $B_{in} \approx 3.2$ , it  
 259 withstands comparison with Fig. 101 [4] where 250 GeV setting is  $B_1 \approx 3.5$  T,  $B_2 \approx 3.25$  T.

260 With these presumably nominal snake and V-to-H / H-to-V rotator settings, spin  $\vec{n}_0$  comes out to be at 11 deg to longitudinal at STAR,  
 261 and at 14.3 deg to vertical at pC-pol (Fig. 95).

262 **Various spin matrices:**

## • STAR to H-Jet

```

263      Spin transfer matrix, momentum group # 1 :
      -4.485796E-02      -2.694575E-02      -0.998630
      2.280418E-02      0.999348      -2.798948E-02
      0.998733      -2.402849E-02      -4.421424E-02

```

## • STAR to PC-POL

```

      -4.656600E-02      -0.976009      0.212693
      -4.794769E-02      -0.210495      -0.976418
      0.997764      -5.566605E-02      -3.699545E-02

```

## 264 • 1-turn spin matrix at IP6

Spin transfer matrix, momentum group # 1 :

```

265      0.926092      0.377148      1.059835E-02
      0.370380      -0.903401      -0.216067
      -7.191486E-02      0.204024      -0.976321

```

```

Determinant =      1.0000000000
Trace =      -0.9536297665; spin precession =      167.6381075517 deg
Precession axis : ( 0.9811, 0.1927, -0.0158)
Spin precession/2pi (or Qs, fractional) :      4.6566E-01

```

266 **5.4 Use spin rotators to manipulate spin  $\vec{n}_0$  at STAR**

267 Store conditions are considered here, beam energy 255 GeV.

268 Spin  $\vec{n}_0$  at STAR is first moved away from vertical. This is done by introducing a perturbation (using SPINR, pure spin rotation, added in  
 269 Yellow at - arbitrarily - IP8; the phase of the spin  $\vec{n}_0$  would change with different location). This perturbation sets the tilt angle at STAR at  
 270 10.53 deg to the vertical Z-axis.

271 Next, the spin rotators are put at work, with matched  $I_{in}$ ,  $I_{out}$  currents to get spin  $\vec{n}_0$  STAR closest to vertical.

272



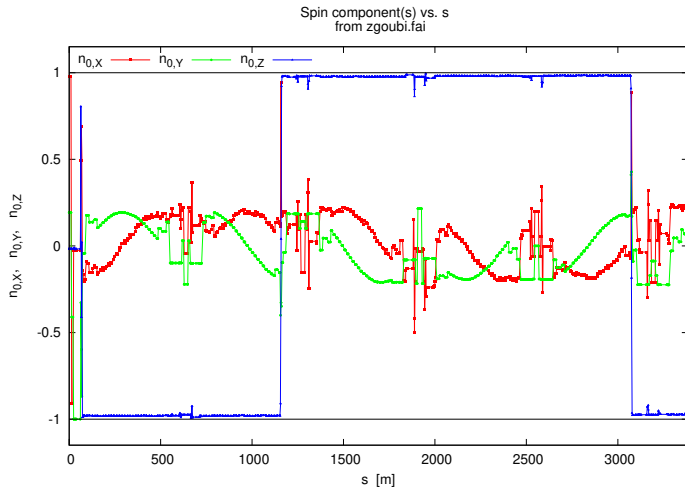


Figure 94: Spin  $\vec{n}_0$  components around yellow, 255.200 GeV. Longitudinal ( $n_{0,x} = 1$ ) in STAR region ( $s=0$ ), mostly vertical elsewhere ( $n_{0,z} = 1$ ). With the present settings (complete snake and nominal rotator settings) the spin tilt from longitudinal at STAR is 11 deg, it is 14.3 deg at pC-polarimeter. The spin component spikes seen on this graph occur at the vertical separation bumps at IPs

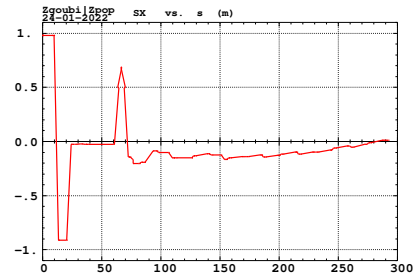
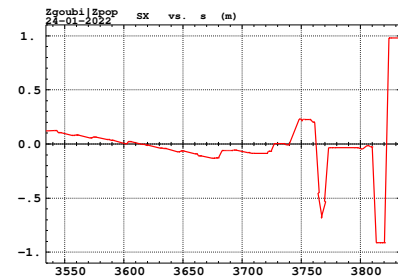


Figure 95: Details of longitudinal spin  $\vec{n}_0$  component in STAR region in yellow, 255.200 GeV.

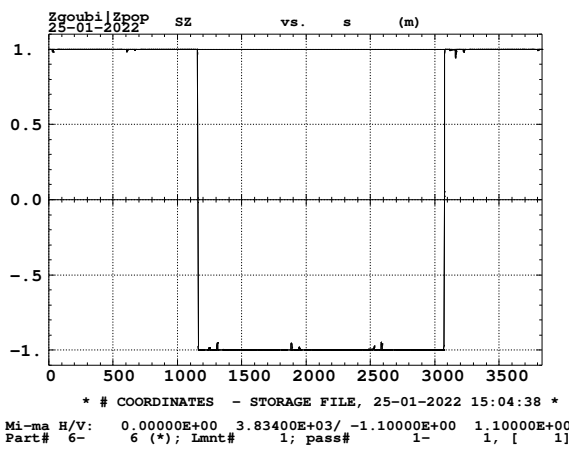


Figure 96: Vertical component of spin  $\vec{n}_0$  around RHIC Yellow. No spin defect, rotators off. Things look almost perfect.

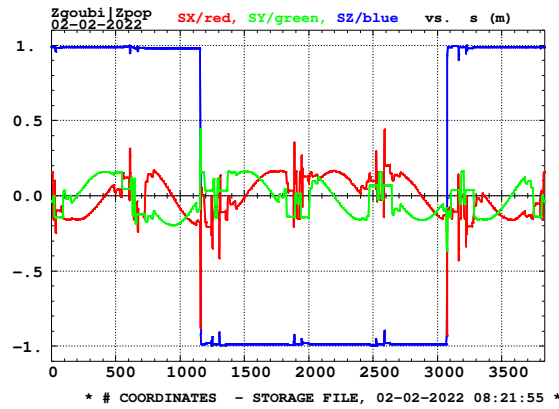


Figure 97: Vertical component of spin  $\vec{n}_0$  around RHIC Yellow. Case of a spin defect (some arbitrary spin rotation, located at IP8 in the present case), rotators off.

283	6	3	44	-500.	151.	150.55203	500.	0.370	SCALING	-	-	
284	6	4	48	-500.	-168.	-167.95000	500.	0.370	SCALING	-	-	
285	STATUS OF CONSTRAINTS (Target penalty = 1.0000E-10)											
286	TYPE	I	J	LMNT#	DESIRED	WEIGHT	REACHED	KI2	NAME	LBL1	LBL2	Nb param. [value]
287	10	1	3	3077	1.000000E+00	1.000E+00	9.999900E-01	1.00E+00	OPTIONS	-	-	0
288	10	1	4	3077	1.000000E+00	1.000E-01	1.000000E+00	0.00E+00	OPTIONS	-	-	0
289	Fit reached penalty value 9.9454E-11											

290 - a tentative with rotator coils coupled:

- 291 - rotatorH2V\_out (36) coupled with rotatorV2H\_out (44): opposite values
- 292 - rotatorH2V\_in (40) coupled with rotatorV2H\_in (48): opposite values
- 293 Vertical angle at STAR mostly unchanged compared to rotators off:

294	STATUS OF VARIABLES (Iteration # 0 / 999 max.)											
295	LMNT	VAR	PARAM	MINIMUM	INITIAL	FINAL	MAXIMUM	STEP	NAME	LBL1	LBL2	
296	6	1	36	-500.	-27.2	-254.96008	500.	1.800E-05	SCALING	-	-	
297	6	1	44	-500.	-27.2	254.96008	500.	1.800E-05	SCALING	-	-	
298	6	2	40	-500.	24.6	370.37000	500.	6.890E-09	SCALING	-	-	
299	6	2	48	-500.	24.6	-370.37000	500.	6.890E-09	SCALING	-	-	
300	STATUS OF CONSTRAINTS (Target penalty = 1.0000E-10)											
301	TYPE	I	J	LMNT#	DESIRED	WEIGHT	REACHED	KI2	NAME	LBL1	LBL2	Nb param. [value]
302	10	1	3	3077	1.000000E+00	1.000E+00	9.825834E-01	1.00E+00	OPTIONS	-	-	0
303	10	1	4	3077	1.000000E+00	1.000E-01	1.000000E+00	0.00E+00	OPTIONS	-	-	0
304	Fit reached penalty value 3.0334E-04											

305 Same result (SZ=0.9825 at STAR) if coupled with same value (rather than opposite signs).

## 6 Spin rotators

A rotator is comprised of 4 modules, with alternating helicities, LRLR in Yellow (going CCW) and RLRL in Blue (going CW) (Fig. 3), field at the ends is radial  $(0, B_Y, 0)$ . A rotator pair allows longitudinal spin orientation at IP, while maintaining spin closed orbit unchanged, *i.e.* vertical, beyond the rotator pair section. The spin angle to the X-axis at exit of a rotator can be anywhere in about  $[0, -180]$  deg, depending on the fields, whereas the rotator axis is in the transverse plane.

### 6.1 Spin rotator field map

The OPERA field maps of the snake modules are all right-handed helices.

A proper transform allows deriving a left-handed helix, as follows. Consider the equations of the field along an helix, to the second order in  $x, y$  they write

$$\begin{cases} B_x/B_0 = \cos(ks)(1 + \frac{k^2}{8}(3x^2 + y^2)) + \frac{k^2}{4}xy \sin(ks) \\ B_y/B_0 = \sin(ks)(1 + \frac{k^2}{8}(x^2 + 3y^2)) + \frac{k^2}{4}xy \cos(ks) \\ B_l/B_0 = -k(x \sin(ks) - y \cos(ks)) \end{cases} \quad (5)$$

with

$$k = \epsilon \frac{2\pi}{\lambda}, \quad \lambda \text{ the pitch period, } \epsilon = \pm 1 \text{ the helicity (+ for right-handed)} \quad (6)$$

$s$  is the distance along the helix axis,  $B_0$  is the peak transverse field value. Here,  $\lambda = 2.4$  m,  $|k| = 2.618$  m<sup>-1</sup>.

Note in passing: given the radial excursions of concern, namely  $x, y < 2$  cm, while  $k^2/8 \approx 1$ , the non-linear terms have negligible contribution to the field.

Consider now reversing the helicity in Eq. 5, *i.e.*  $k \rightarrow -k$ , thus the field changes to

$$\begin{cases} {}^r B_x/B_0 = \cos(ks)(1 + \frac{k^2}{8}(3x^2 + y^2)) - \frac{k^2}{4}xy \sin(ks) \\ {}^r B_y/B_0 = -\sin(ks)(1 + \frac{k^2}{8}(x^2 + 3y^2)) + \frac{k^2}{4}xy \cos(ks) \\ {}^r B_l/B_0 = -k(x \sin(ks) + y \cos(ks)) \end{cases} \quad (7)$$

By changing  $s \rightarrow -s$  in Eq. 5, the very expressions  ${}^r B_x/B_0$  and  ${}^r B_y/B_0$  of Eq. 7 are obtained, while it yields  $-{}^r B_l/B_0$  instead. In conclusion, a left-handed field map can be obtained by a backward read/write of the right-handed helix field map, with a change of sign of the longitudinal component. A  $\pi/2$  rotation has to follow as the field at entrance of the rotators is radial.

Rotator currents do not exceed 220 Amp in principle, so assume this is still about linear regime and take the low-field snake module field map (it has been computed for 100 Amp, whereas high field snake module field maps were computed for 322 Amp). The file maps of both left-handed and right handed modules are available at

<https://sourceforge.net/p/zgoubi/code/HEAD/tree/trunk/exemples/RHIC/rotatorsWithFieldMaps/fieldmaps/>

Tracking results using that rotator field map are given in Figs. 98-100, The magnetic field through the rotator fairly agrees with Fig. 2 in [4] (Fig. 101).

The input data file for the L+R+L+R+ snake module series is given as an example in App. B. The input files of all four rotator species (Fig. 3) are available at

<https://sourceforge.net/p/zgoubi/code/HEAD/tree/trunk/exemples/RHIC/rotatorsWithFieldMaps/examples/rotators/>

Yellow CW with spin rotators and snakes is available at

[https://sourceforge.net/p/zgoubi/code/HEAD/tree/trunk/exemples/RHIC/rotatorsWithFieldMaps/examples/RHIC\\_Yellow\\_withSnakesAndRotators/](https://sourceforge.net/p/zgoubi/code/HEAD/tree/trunk/exemples/RHIC/rotatorsWithFieldMaps/examples/RHIC_Yellow_withSnakesAndRotators/)

README files in these various sourceforge folders give some guidance regarding the content of these files, and the way to use them.

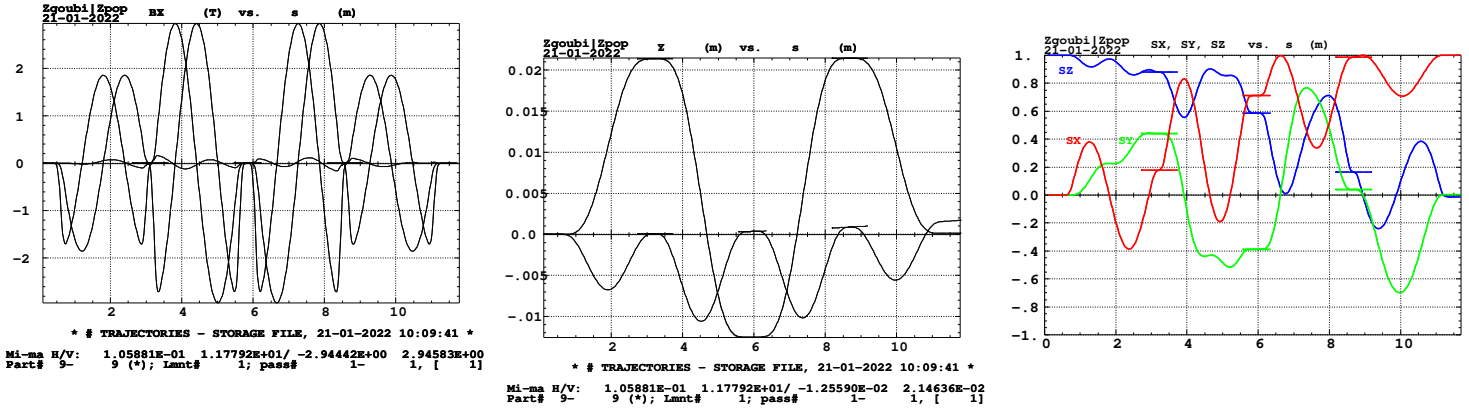


Figure 98: Field components along L+R+L+R+ rotator, for 90 deg rotation (this is close to injection energy case, where 25 GeV. Z-rotation by D0 and DX is only 10 deg).  
 Figure 99: H and V losed orbit coordinates  
 Figure 100: Spin components. Starting vertical, spin moves to longitudinal.

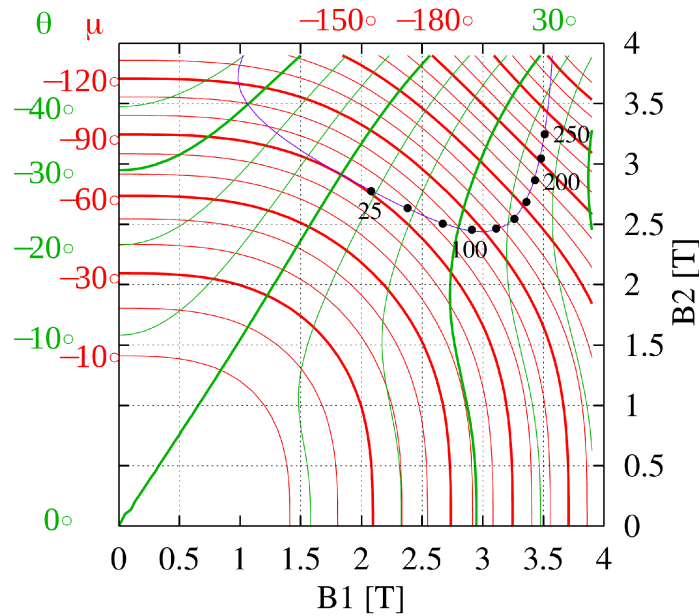


Figure 101: From Ref. [4]. Field dependence of the spin precession angle ( $\mu$ ) and precession axis angle to the radial axis ( $\theta$ ; the precession axis is in the transverse plane).  $B_1$  and  $B_2$  are field values in respectively the outer and inner pair of coils. 25 to 250 GeV set points (black dots) compare well with present simulation outcomes.

## 342 Appendix

## 343 A Optical sequences for 2-coil 9 o'clock and full 3 o'clock snakes

344 A few regular optical elements upstream and downstream of the field map sequences are added, in order to clarify the insertion of the latter  
 345 amongst an optical elements sequence translated from the MADX model of RHIC Blue ring.

346 Left column below: coils 1&3 configuration (for 1&4 coils case, permute the 3rd and 4th TOSCA keywords). Right column: full 3 o'clock  
 347 snake, nominal settings [2].

348

```
'MULTIPOL'      BI9_QD  8
'DRIFT'         DRIFT_80
29.610500
'DRIFT'        MONI      BI9_B8
0.000000
'MARKER'       ERHLX
'DRIFT'        snakSS_up
131.741795

'MARKER'       START SNK1
'DRIFT'        -78.200000

'DRIFT'
3.600000
'DRIFT'
16.400000

'TOSCA'        snk1HighB
0 0000 ! .plt
-3.000000000E+02  1.0 1.0 1.0
HEADER_8      RHIC_helix
361 81 81 15.1 0.246305418719e-4  ! = 1/4.060e4
b_model13a2a322a-x-4_4_y-4_4_z-180_180-integral.table
0 0 0 0
2
.1
2 0.000000000E+00 0.000000000E+00 0.000000000E+00

'DRIFT'        2.162m_C1toC2
-98.800000

'TOSCA'        snk1HighB
0 0000 ! .plt
-1.00275297E-13  1.0 1.0 1.0
HEADER_8
361 81 81 15.1 1.
b_model13a2a322a-x-4_4_y-4_4_z-180_180-integral.table
0 0 0 0
2
.1
2 0.000000000E+00 0.000000000E+00 0.000000000E+00

'DRIFT'        2.162m_C2toC3
-75.200000

'TOSCA'        snk1HighB
0 0000 ! .plt
3.000000000E+02  1.0 1.0 1.0
HEADER_8      RHIC_helix
361 81 81 15.1 0.246305418719e-4  ! = 1/4.060e4
b_model13a2a322a-x-4_4_y-4_4_z-180_180-integral.table
0 0 0 0
2
.1
2 0.000000000E+00 0.000000000E+00 0.000000000E+00

'DRIFT'        2.162m_C3toC4
-98.800000

'TOSCA'        snk1HighB
0 0000 ! .plt
1.000000000E-10  1.0 1.0 1.0
HEADER_8      RHIC_helix
361 81 81 15.1 0.246305418719e-4  ! = 1/4.060e4
b_model13a2a322a-x-4_4_y-4_4_z-180_180-integral.table
0 0 0 0
2
.1
2 0.000000000E+00 0.000000000E+00 0.000000000E+00

'DRIFT'
16.400000

'DRIFT'
-78.200000

! END SNAKE 1

'DRIFT'        snakSS_dw
131.741795
'MARKER'       ERHLX
'DRIFT'        MONI      BI9_B7
0.000000
'DRIFT'        DRIFT_82
29.623400
'MULTIPOL'     BI9_QF  7
```

```
'MULTIPOL'      BO3_QF  8
'DRIFT'         DRIFT_80
29.610500
'DRIFT'        MONI      BO3_B8
0.000000
'MARKER'       ERHLX
'DRIFT'        snak2SS_up
131.741795

'MARKER'       START SNK2
'DRIFT'        -78.200000

'DRIFT'
3.600000
'DRIFT'
16.400000

'TOSCA'
0 000 ! .plt
-1.000000000E+02  1.0 1.0 1.0
HEADER_8      RHIC_helix
361 81 81 15.1 0.748502994012e-4  ! = 1/1.3360e4
b_model13a2a-x-4_4_y-4_4_z-180_180-integral.table
0 0 0 0
2
.1
2 0.000000000E+00 0.000000000E+00 0.000000000E+00

'DRIFT'        2.162m_C1toC2
-98.800000

'TOSCA'
0 000 ! .plt
3.220000000E+02  1.0 1.0 1.0
HEADER_8      RHIC_helix
361 81 81 15.1 0.246305418719e-4  ! = 1/4.060e4
b_model13a2a322a-x-4_4_y-4_4_z-180_180-integral.table
0 0 0 0
2
.1
2 0.000000000E+00 0.000000000E+00 0.000000000E+00

'DRIFT'        2.162m_C2toC3
-75.200000

'TOSCA'
0 000 ! .plt
-3.220000000E+02  1.0 1.0 1.0
HEADER_8      RHIC_helix
361 81 81 15.1 0.246305418719e-4  ! = 1/4.060e4
b_model13a2a322a-x-4_4_y-4_4_z-180_180-integral.table
0 0 0 0
2
.1
2 0.000000000E+00 0.000000000E+00 0.000000000E+00

'DRIFT'        2.162m_C3toC4
-98.800000

'TOSCA'
0 000 ! .plt
1.000000000E+02  1.0 1.0 1.0
HEADER_8      RHIC_helix
361 81 81 15.1 0.748502994012e-4  ! = 1/1.3360e4
b_model13a2a-x-4_4_y-4_4_z-180_180-integral.table
0 0 0 0
2
.1
2 0.000000000E+00 0.000000000E+00 0.000000000E+00

'DRIFT'
16.400000

'DRIFT'
-78.200000

! END SNAKE 2

'DRIFT'        snak2SS_dw
131.741795
'MARKER'       ERHLX
'DRIFT'        MONI      BO3_B7
0.000000
'DRIFT'        DRIF      DRIFT_82
29.623400
'MULTIPOL'     BO3_QD  7
```

350 **B Optical sequence of a spin rotator**351 This is the case of L+R+L+R+: from arc to IP6 (vertical to longitudinal  $\vec{n}_0$ ) in Yellow, going CCW.

```

L+R+L+R+ rotator:
! arc to IP, V to H spin, along Yell 7 o'clock CCW.
'OBJET'
851.249816894531 * 1.d3
1
2
4 1
0.00000000E+00 0.00000000E+00 0.00000000E+00 0.00000000E+00 0.00 1.00000000E+00 'o'
0.00000000E+00 0.00000000E+00 0.00000000E+00 0.00000000E+00 0.00 1.00000000E+00 'o'
0.00000000E+00 0.00000000E+00 0.00000000E+00 0.00000000E+00 0.00 1.00000000E+00 'o'
0.00000000E+00 0.00000000E+00 0.00000000E+00 0.00000000E+00 0.00 1.00000000E+00 'o'
1 1 1 1
'PARTICUL'
PROTON
'SPNTRK'
4
1.00000000E+00 0.00000000E+00 0.00000000E+00
0.00000000E+00 1.00000000E+00 0.00000000E+00
0.00000000E+00 0.00000000E+00 1.00000000E+00
0.00000000E+00 0.00000000E+00 1.00000000E+00
'SCALING'
1 2
TOSCA rotatorH2V_o* ! goes horiz to vert
-1
263.68537
1.
TOSCA rotatorH2V_i*
-1
213.77669
1.
'MARKER' R+L+R+L+_S
5
'DRIFT' rotator_adjL
71.836840
6
'TOSCA' rotatorH2V_out_L+
7
0 0020 ! .plt
1.00000000E+00 1.00000000E+00 1.00000000E+00 1.00000000E+00
HEADER_8 RHIC_helix
361 81 81 15.1 0.748502994012e-4 ! = 1/1.3360e4
b_rotatorModule_leftHanded.table
0 0 0 0
2
.3
2 0.00000000E+00 0.00000000E+00 0.00000000E+00
'DRIFT'
-98.800000
8
'TOSCA' rotatorH2V_in_R+
9
0 0020 ! .plt
1.00000000E+00 1.00000000E+00 1.00000000E+00 1.00000000E+00
HEADER_8 RHIC_helix
361 81 81 15.1 0.748502994012e-4 ! = 1/1.3360e4
b_rotatorModule_rightHanded.table
0 0 0 0
2
.3
2 0.00000000E+00 0.00000000E+00 0.00000000E+00
'DRIFT'
-75.200000
10
'DRIFT'
35.889200
11
'DRIFT'
-35.889200
12
'TOSCA' rotatorH2V_in_L+
13
0 0020 ! .plt
1.00000000E+00 1.00000000E+00 1.00000000E+00 1.00000000E+00
HEADER_8 RHIC_helix
361 81 81 15.1 0.748502994012e-4 ! = 1/1.3360e4
b_rotatorModule_leftHanded.table
0 0 0 0
2
.3
2 0.00000000E+00 0.00000000E+00 0.00000000E+00
'DRIFT'
-98.800000
14
'TOSCA' rotatorH2V_out_R+
15
0 0020 ! .plt
1.00000000E+00 1.00000000E+00 1.00000000E+00 1.00000000E+00
HEADER_8 RHIC_helix
361 81 81 15.1 0.748502994012e-4 ! = 1/1.3360e4
b_rotatorModule_rightHanded.table
0 0 0 0
2
.3
2 0.00000000E+00 0.00000000E+00 0.00000000E+00
'DRIFT' rotator_adjL
71.836840
16
'MARKER' R+L+R+L+_E
17
'FIT2'
2
4 4 0 2.
4 8 0 2.
2 1e-12
10 4 3 #End 0. 1. 0
10 4 4 #End 1. .1 0
'FAISCEAU'
'SPNPRT' MATRIX
19
'END'
20

```

## References

- [1] H. Huang et al.: Polarized Proton Acceleration at the Brookhaven AGS and RHIC. Presentation slides, PAC 03 Accelerator Conference (May 12, 2003).  
<https://accelconf.web.cern.ch/p03/PAPERS/MOPA009.PDF>  
H. Huang: Minutes of 2003/4/16, 8:30 meeting.
- [2] F. Méot, Gupta, R., Huang, H., Ranjbar, V., Robert-Demolaize, G.: Re-visiting RHIC snakes: OPERA fields,  $\vec{n}_0$  dance. C-A/AP/590; BNL-114379-2017-IR (Sept. 2017).  
<https://technotes.bnl.gov/PDF?publicationId=42159>
- [3] F. Méot: Spinor Algebra. USPAS 2021 Summer Spin Class Proceedings. To be published by Springer (2022).  
Slides: <https://uspas.fnal.gov/materials/21onlineSBU/Spin-Dynamics/Lectures/Lecture%204-Spinor%20Methods.pdf>
- [4] W. MacKay, et als.: Commissioning spin rotators in RHIC. Proceedings of the 2003 Particle Accelerator Conference.